Emerging Roles of Importin α/β and EB1 in Differential Regulation of Kif18B Astral Microtubule Destabilization

[1]Sanjay Shrestha, [1]Stephanie C. Ems-McClung, [1*]Mark A. Hazelbaker, [1#]Amber L. Yount, [2]Sidney L. Shaw, and [1]Claire E. Walczak

[1]Medical Sciences, Indiana School of Medicine – Bloomington, 915 E. Third Street, Bloomington, IN 47405

[2]Department of Biology, Indiana University, 915 E. Third Street, Bloomington, IN 47405

Running Head: Importins and EB1 modulate Kif18B

*Present Address:

Mark A. Hazelbaker
Dept. of Cell Biology and Physiology
111 Mason Farm Road
5200 Medical Biomolecular Research Building CB #7545
Chapel Hill, NC 27599-7545

#Present Address:

Amber L. Yount
Dept. of Biology
Franklin College
101 Branigin Blvd
Franklin, IN 46131

Abstract

Tight regulation of microtubule dynamics and microtubule organization is necessary for proper spindle assembly and chromosome segregation. The microtubule destabilizing Kinesin-8, Kif18B, controls astral microtubule dynamics and spindle positioning. Kif18B interacts with importin α/β as well as with the plus-tip tracking protein EB1, but how these associations modulate Kif18B activity or function is not known. We mapped the key binding sites on Kif18B, made residue-specific mutations, and assessed their impact on Kif18B function. Blocking EB1 interaction disrupted Kif18B MT plus-end accumulation and inhibited its ability to control astral microtubule length in cells. Blocking importin α/β interaction reduced Kif18B plus-end accumulation on astral MTs but did not inhibit its ability to control astral MT length. *In vitro*, importin α/β increased Kif18B binding to the microtubule lattice, which enhanced Kif18B accumulation at microtubule plus ends, and stimulated microtubule destabilization, suggesting that the importins spatially regulate Kif18B. In contrast, EB1 promoted microtubule destabilization without increasing lattice binding *in vitro*, which suggests that EB1 and importin α/β have distinct roles in the regulation of astral microtubule dynamics. We propose that Ran-regulation is important not only to control motor function near chromatin but also provides a spatial control mechanism to modulate microtubule binding of NLS-containing spindle assembly factors.

Introduction

The mitotic spindle is a macromolecular machine composed of dynamic microtubules (MTs) and associated proteins responsible for segregation of the chromosomes during mitosis. Proper spindle assembly requires tight spatial and temporal control of MT dynamics and organization that is governed in part by the RanGTP gradient (Kalab and Heald, 2008). RanGTP is high in the vicinity of chromosomes and dissipates steeply toward the spindle poles (Kalab *et al.*, 2002; Caudron *et al.*, 2005; Kalab *et al.*, 2006). RanGTP modulates the activity of multiple spindle assembly factors through the nuclear transport receptors importin α/β, which bind to proteins containing a nuclear localization signal (NLS) (Kalab and Heald, 2008). In regions where RanGTP is high, RanGTP binds to importin β, causing a conformational change, which induces release of the cargo from importin α, allowing that cargo protein to be activated locally within the spindle. Ran-regulated targets include molecular motor proteins that help organize the spindle MT arrays, as well as a number of proteins that regulate spindle MT dynamics (Gruss *et al.*, 2001; Wiese *et al.*, 2001; Trieselmann *et al.*, 2003; Ems-McClung *et al.*, 2004; Ribbeck *et al.*, 2006; Sillje *et al.*, 2006; Tahara *et al.*, 2008).

Members of both the Kinesin-13 and Kinesin-8 families of molecular motors play critical roles in controlling MT dynamics (Walczak *et al.*, 2013). The Kinesin-13 proteins are strictly MT depolymerizing enzymes (Desai *et al.*, 1999), whereas the Kinesin-8 proteins are MT plus-end directed motors and MT plus-end destabilizing enzymes (Gupta *et al.*, 2006; Varga *et al.*, 2006). The yeast Kinesin-8, Kip3p, can directly depolymerize stabilized MTs in a length dependent manner (Varga *et al.*, 2006), albeit less robustly than the Kinesin-13 proteins, but the vertebrate Kinesin-8 proteins, Kif18A, Kif18B, and Kif19A have more subtle effects (Mayr *et al.*, 2007; Du *et al.*, 2010; Niwa *et al.*, 2012; Shin *et al.*, 2015; McHugh *et al.*, 2018). During mitosis, Kif18A is enriched on kinetochores and is important in controlling chromosome oscillations (Stumpff *et al.*, 2008). Analysis of the purified protein suggests that it may have weak MT destabilization activity (Mayr *et al.*, 2007) but most likely acts as a capping protein (Du *et al.*, 2010). Kif18B localizes to the plus ends of astral MTs (Lee *et al.*, 2010) and is important in controlling astral MT dynamics (Stout *et al.*, 2011; Tanenbaum *et al.*, 2011; Walczak *et al.*, 2016; McHugh *et al.*, 2018) and spindle positioning (McHugh *et al.*, 2018; Moreci and Lechler, 2021). Full-length Kif18B protein could not depolymerize stabilized MTs, but a truncated derivative lacking the C-terminal tail had weak MT depolymerization activity (McHugh *et al.*, 2018).

The mechanisms by which Kif18B modulates MT dynamics are likely complex due to the interaction of its tail domain with multiple binding partners in a spatially regulated manner. Kif18B binds directly to EB1, and its localization to astral MT plus-ends is diminished in EB1 knockdown cells (Stout *et al.*, 2011; Tanenbaum *et al.*, 2011). In contrast, EB1 localization is not affected by Kif18B knockdown (Stout *et al.*, 2011; Tanenbaum *et al.*, 2011). Consistent with that finding, Kif18B is not uniformly colocalized with EB1, which is found on all MT plus-ends, and is instead enriched on astral MTs near the cortex (Stout *et al.*, 2011; Tanenbaum *et al.*, 2011; van Heesbeen *et al.*, 2017). Super-resolution imaging of mammalian cells showed two spatially resolved localization patterns of Kif18B on astral MTs. While Kif18B and EB1 colocalized on astral MTs closer to the poles, a subset of Kif18B was localized distally to EB1 by 189 nm on astral MTs near the cortex in the vicinity of the metaphase plate (Stout *et al.*, 2011b; Shin *et al.*, 2015). Further evidence of spatial regulation of Kif18B is provided by lifetime imaging of MTs in PtK2 cells depleted of Kif18B. Analysis of EB1 MT plus-tip dynamics

in these cells showed that MTs in the polar region near the cortex had reduced dynamics compared to those MTs above and below the spindle (Walczak *et al.*, 2016).

In addition to binding EB1, Kif18B has multiple other binding partners. Kif18B physically interacts with MCAK at astral MT ends (Tanenbaum *et al.*, 2011), where Kif18B and MCAK may coordinately modulate astral MT dynamics. The tail of Kif18B also binds to importin α/β (Stout *et al.*, 2011b), but whether this binding is utilized simply for nuclear localization or whether Kif18B is another Ran-regulated factor is not known. One possibility is that Kif18B is spatially regulated through the RanGTP network. However, this creates a paradox because the RanGTP gradient is thought to act locally around the chromosomes, yet Kif18B localization is most prominent near the cortex. The MT destabilization activity of Kif18B is proposed to be important for modulating MT forces between the cortex and spindle poles that impact spindle positioning and spindle bipolarization (van Heesbeen *et al.*, 2017; McHugh *et al.*, 2018; Moreci and Lechler, 2021). The Kif18B tail also contains a second MT binding site that is important in modulating both diffusion and processivity of the motor on MTs (Shin *et al.*, 2015; McHugh *et al.*, 2018). Deletion of the tail disrupts plus-end localization in cells (Stout *et al.*, 2011b; McHugh *et al.*, 2018), which is mediated by increases in the off-rate from MTs, reduction in the run length of the motor on the MT, and reduction of the motor dwell time at MT ends, despite increased motor velocities (Shin *et al.*, 2015; McHugh *et al.*, 2018). Previous studies using computer simulations of how a MT destabilizer affects MT dynamics indicate that on-rate, processivity, and off-rate at MT plus-ends are critical factors for reducing MT length (Weaver *et al.*, 2011). Thus, Kif18B tail-mediated MT and plus end binding appear to be key for Kif18B function, which we propose is modulated differentially by its interactors, importin α/β and EB1.

In this study we developed a series of inter-molecular FRET reporters to precisely map the individual binding sites of Kif18B with both importin α and EB1. We found that importin α/β and EB1 compete for binding to the Kif18B tail, and that importin α/β increase plus-end binding of Kif18B by loading Kif18B onto the MT lattice with subsequent plus-end localization where it reduces MT length. In contrast, EB1 reduces MT length without increasing overall Kif18B MT binding. Consistent with the effects of EB1 knockdown regulating Kif18B localization in cells, we show that the specific interaction of Kif18B with EB1 is critical for MT plus-end localization and regulation of astral MT length in monopolar spindles. On the other hand, blocking the interaction of Kif18B with importin α/β by mutation of the NLS does not hinder the ability of Kif18B to control astral MT length in monoasters but does prevent bipolar spindle formation when it is overexpressed. Most notably, the NLS mutations compromise the plus-end accumulation of Kif18B on astral MTs, consistent with importin α/β spatially regulating Kif18B localization. We propose that Ran-regulation is important not only to control motor function near chromatin but that the Ran-system is an overall spatial control mechanism to control MT binding affinity of MT associated proteins.

Results

Kif18B Tail Interacts with Importin α/β, EB1, and Microtubules

Kif18B has an N-terminal kinesin catalytic domain, a central stalk region, and a C-terminal tail that has two putative nuclear localization signal (NLS) sequences, one non-canonical bipartite and one monopartite, and three putative EB1 binding domains (EBBD) (Figure 1A) {Lee, 2010 #2066(Stout *et al.*, 2011b; Tanenbaum *et al.*, 2011). To understand how Kif18B interacts with its different binding partners, we designed a series of Förster resonance energy transfer (FRET) reporters to look at protein-protein interactions. Either importin α or EB1 were fused to CyPet as donors, and the Kif18B tail was fused to YPet as the acceptor (Figures, 1B and S1). In addition to the full-length tail (aa 605-828), we also generated two tail fragments (aa 605-707 and aa 708-828) to separate the putative NLS and EBBD sites (Figure 1C). To test interactions between the Kif18B tail and importin α, we incubated importin α-CyPet + importin β with increasing molar concentrations of YPet-Kif18B(605-828), YPet-Kif18B(605-707), or YPet-Kif18B(708-828) and measured FRET (Figures, 1D and S1A). Importin α-CyPet induced FRET with all three YPet-Kif18B tail fragments, suggesting that the tail of Kif18B contains at least two independent importin α binding domains. Addition of RanQ69L to importin α-CyPet/importin β and YPet-Kif18B tail proteins disrupted their interaction as seen by a reduction in their FRET ratio, demonstrating Ran regulation of these interactions (Figure S1B). Incubation of EB1-CyPet with increasing molar concentrations of the YPet-Kif18B tail fragments resulted in a dose-dependent increase in FRET with each tail fragment, suggesting that the Kif18B tail also has at least two independent EB1 binding domains (Figures, 1E and S1C).

The putative NLS and EBBD sites are juxtaposed to one another in the tail of Kif18B (Figure 1A). To ask whether the interaction of the Kif18B tail with importin α/β and EB1 is competitive, YPet-Kif18B tail fragments were incubated with EB1-CyPet and a four-fold molar excess of unlabeled importin α/β relative to EB1-CyPet, and the FRET ratio was effectively reduced (Figure 1F, left), indicating that there is competition for binding between EB1 and importin α/β to the tail of Kif18B. In contrast, when YPet-Kif18B fragments were added to importin α-CyPet/importin β and a four-fold molar excess of unlabeled EB1, EB1 was unable to compete with importin α/β for binding to the tail of Kif18B (Figure 1F, right). Thus, the discrepancy between the reciprocal experiments may be a consequence of different affinities.

Members of the Kinesin-8 family have an ATP-independent MT binding domain in the tail that is important for motor binding and processivity as well as for MT cross-linking (Stumpff *et al.*, 2011; Su *et al.*, 2011; Weaver *et al.*, 2011b; McHugh *et al.*, 2018). To assess Kif18B tail MT binding, we carried out MT pelleting assays in which YPet-Kif18B(605-828) was incubated with increasing amounts of MTs in the presence or absence of importin α/β or EB1 (Figure 1G). Addition of importin α/β resulted in a mild and non-significant 20% reduction in the maximal binding of the tail to MTs but resulted in a 17-fold increase in the K_d for MTs ($p<0.0001$) (left); whereas addition of EB1 had no effect on maximal binding nor on the K_d (Figure 1G, right). These results suggest that importin α/β may modulate Kif18B MT binding or processivity through the tail.

Kif18B Contains Two NLS Sites that Mediate Interaction with Importin α/β

To identify the critical residues for binding to importin α/β, we mutated both halves of the bipartite NLS by changing the basic residues to alanine residues (NLS1) or mutated all four basic residues of the monopartite NLS to alanine residues (NLS2) (Figure 2A) and tested them for interaction with importin α/β in the FRET assay (Figure 2B). Mutation of NLS1 in YPet-Kif18B(605-707) and mutation of NLS2 in YPet-Kif18(708-828) reduced the FRET ratio when incubated with importin α-CyPet/importin β. Mutation of both NLS1 and NLS2 (NLS1/2) also reduced the FRET ratio of YPet-Kif18B(605-828) with importin α-CyPet/importin β (Figure 2B) to the same level as mutation of the NLS in each half of the tail, suggesting there are two functional NLS sites in the tail of Kif18B.

Because of the complex interactions of the Kif18B tail with its different binding partners, we wanted to make sure that mutation of the NLS regions did not impair binding to EB1 or MTs, which would complicate interpretations of functional experiments. The NLS1/2 mutations in YPet-Kif18(605-828) did not impair interaction with EB1-CyPet, but slightly increased their interaction (Figure 2C). However, the NLS1/2 mutations caused ~50% reduction in maximal MT binding and ~4-fold increase in the K_d for MT binding relative to YPet-Kif18B(605-828) (Figures, 1G and 2D), suggesting a moderate effect on MT affinity. Interestingly, these results are similar to our previous work with the Kinesin-14 XCTK2, wherein importin α/β regulate the interaction of the XCTK2 tail with MTs to control its ability to cross-link MTs (Ems-McClung *et al.*, 2004; Ems-McClung *et al.*, 2020), suggesting a common regulatory mechanism for importin-regulated MT binding of kinesin tails.

Kif18B Contains Two EB1 Binding Domains

To identify the critical residues for binding to EB1, we mutated the critical leucine and proline residues (LP) in the EB1 SXIP binding motif (Honnappa *et al.*, 2009) to asparagine (NN) and tested the wild type and mutant constructs for their ability to interact with EB1-CyPet using the FRET assay (Figure 3, A and B). Mutation of E1 in YPet-Kif18B(605-707), and mutation of E3 in YPet-Kif18(708-828) reduced the FRET ratio when incubated with EB1-CyPet (Figure 3B, left), whereas mutation of E2 in YPet-Kif18(708-828) had no effect (Figure 3B, right). Mutation of both E1 and E3 together reduced the FRET ratio of YPet-Kif18B(605-828) with EB1-CyPet to levels similar to either E1 or E3 in their respective tail fragments (Figure 3B, left). These results suggest that Kif18B has two separate EB1 binding domains in its tail.

To test whether mutation of the EBBDs impaired binding to the other partners, we tested the interaction of the EBBD mutated Kif18B(605-828) tail with each of its binding partners (Figure 3, C and D). Mutation of E1/3 in YPet-Kif18(605-828) did not impair interaction with importin α-CyPet/importin β (Figure 3C), nor did it affect its binding to MTs (Figures, 1G and 3D). Together our data show that the tail of Kif18B contains distinct binding sites to mediate interactions with importin α/β and MTs, and with EB1.

Interaction with Importin α/β and EB1 are Important for Proper Kif18B Localization on MT Ends and to Modulate Astral MT Dynamics in Cells

To ask whether disruption of the interaction of Kif18B with importin α/β or with EB1 impacts its ability to modulate MT dynamics in cells, we knocked down Kif18B in HeLa cells, transduced the cells with lentiviral

wild-type (WT) GFP-Kif18B or GFP-Kif18B with the NLS1/2 (NLS) or EBBD1/3 (EBBD) mutations, and treated the cells with Monastrol to induce monopolar spindles (Figure 4A, Figure S2A). Kif18B clearly localized to the tips of astral MTs in control cells (Figure 4A, row 1). This staining was abolished in cells with Kif18B knockdown and resulted in an increase in the MT aster area (Figure 4A, row 2), consistent with previous results {Walczak, 2016 #2497}. Lentiviral expressed WT GFP-Kif18B localized to astral MT plus-ends like the endogenous Kif18B and reduced the MT aster size (Figure 4A, row 3). Mutation of the NLS in Kif18B reduced MT plus tip localization and reduced MT aster size (Figure 4A, row 4). In contrast, mutation of the EBBD nearly abolished localization of Kif18B to the plus tips of MTs and did not reduce MT aster size (Figure 4A, row 5). When comparing the GFP-Kif18B expression level to MT aster size, we noted that for both the WT and NLS mutant, there was a robust negative correlation (Figure S2, B and C) compared to a weaker correlation for the EBBD mutant (Figure S2D). The inability of the EBBD mutant to reduce the aster size and its reduced correlation of expression level with aster size suggests that disruption of the interaction with EB1 impacted the ability of Kif18B to destabilize MTs. When analyzing the population of the transduced cells, we noted that the expression levels varied significantly between WT and mutant proteins (Figure S2E). To rule out the possibility that the reduced ability of the GFP-Kif18B EBBD mutant to rescue aster size was due to lower expression levels, we determined the range of expression levels of WT GFP-Kif18B that was able to fully rescue aster size (Figure 4B). We then identified cells transduced with mutant Kif18B NLS and EBBD proteins with a similar range of GFP expression and compared their MT aster area (Figure 4, B and C). Knockdown of Kif18B resulted in a 35% increase in aster area compared to control knockdown with mock expression (Figure 4C). Expression of WT GFP-Kif18B or GFP-Kif18B NLS was able to fully rescue aster area, but GFP-Kif18B EBBD was only able to partially rescue aster area (Figure 4C). These results suggest that while disrupting the interaction of Kif18B with importin α/β disrupts its ability to robustly localize to MT plus-ends, this is not sufficient to impact its ability to control MT aster size. Consistent with previous findings (Stout *et al.*, 2011; Tanenbaum *et al.*, 2011), our results confirm that interaction of Kif18B with EB1 is necessary both for localization to MT plus-ends and to control MT length in mitotic asters.

When examining the mitotic figures in Monastrol-arrested cells after knockdown/rescue of Kif18B, we noticed a dramatic increase in the percentage of bipolar spindles in cells expressing high levels of WT GFP-Kif18B (Figure 5, A and B). Most control cells or cells in which Kif18B was knocked down and mock rescued had very few bipolar spindles (<5%), as would be expected for Monastrol-arrested cells (Figure 5B). In contrast, Kif18B knockdown cells overexpressing WT GFP-Kif18B and treated with Monastrol had ~50% bipolar spindles (Figure 5B). These results suggest that increased MT dynamics by overexpressed Kif18B on the astral MTs promoted spindle bipolarization, which is consistent with previous studies showing that Kif18B is needed for bipolar spindle assembly in Eg5 independent cells. This role of Kif18B was proposed to be due to Kif18B regulating astral MT dynamics near the cortex and impacting cortical pulling forces that impact centrosome separation (van Heesbeen *et al.*, 2017). Unlike in WT rescued cells, we did not observe dramatic increases in the bipolar spindles in cells overexpressing NLS or EBBD mutants (Figure 5B). The inability of the mutant Kif18B proteins to induce spindle bipolarization was not due to variation in expression level, as the expression of WT GFP-Kif18B and the two mutants were similar in the Kif18B knockdown cells (Figure 5C).

These results suggest that while mutation of the NLS does not disrupt the ability of Kif18B to control the length of astral MTs in monopolar spindles, it does impair the ability of overexpressed Kif18B to induce bipolar spindle assembly in Monastrol-treated cells.

Importin α/β Controls the Spatial Distribution of Kif18B in Monopolar Spindles

When examining the monopolar spindles in the knockdown/rescue experiments, we noted that the NLS mutant appeared to have reduced plus tip localization compared to WT GFP-Kif18B. This observation raised the idea that the interaction with importin α/β may impact the spatial localization of Kif18B. We used 3D-SIM to analyze the localization of lentiviral expressed WT and NLS mutant GFP-Kif18B to MT ends in monopolar spindles of cells depleted of endogenous Kif18B (Figure S3A). Whereas WT GFP-Kif18B localized robustly to the plus ends of MTs near the cortex (Figure S3A, left), the NLS mutant had overall reduced MT plus-end localization (Figure S3A, right). To test the idea that proper Ran regulation contributes to the spatial distribution of Kif18B, we treated Monastrol-arrested cells with the drug importazole that disrupts importin α/β interaction with NLS containing proteins (Soderholm *et al.*, 2011), stained the cells with Kif18B and EB1 antibodies, and imaged them using 3D-SIM (Figure S3B). Like mutation of the NLS site in GFP-Kif18B, importazole treatment compromised the localization of endogenous Kif18B on the astral MTs, effectively disrupting the plus end localization. The NLS mutant localization and the results from importazole treatment support the idea that the Ran gradient, through importin α/β, spatially regulates Kif18B localization to MTs.

Importin α/β Increases Kif18B Association with MTs to Enhance MT Destabilization Activity

To understand how the interaction of Kif18B with importin α/β and EB1 affects the ability of Kif18B to localize to MTs and alter MT dynamics, we expressed and purified full-length WT GFP-Kif18B, added it to *in vitro* polarity marked dynamic MTs in the absence and presence of excess importin α/β or EB1, and analyzed both the motor binding events and MT lengths using a custom-built MATLAB algorithm (Figures, 6A and S4A). Previous studies have shown that the plus ends of dynamic MTs assemble tubulin approximately three-folder faster than the minus end (Mitchison and Kirschner, 1984); thus, when stabilized MT seeds are added to a solution of tubulin-GTP, MTs assemble from both ends of the seed to different lengths, resulting in the long plus-end extensions having on average three-fold longer MT extensions than the short minus-end extensions (Kristofferson *et al.*, 1986). We visualized this difference in polarity by polymerizing the seeds with Cy5-tubulin (gray) and the MT extensions with X-rhodamine tubulin (magenta) (Figure 6A). Assembling polarity-marked MTs resulted in four classes of MTs: seed only, seed with one extension (1-sided), seed with two extensions (2-sided), and extension only (Figure S4A). Because Kif18B is a plus-end directed motor and to confidently assess Kif18B effects on MT binding and length, we only analyzed MTs with two extensions of differing lengths (2-sided) in which we assigned the long extension as the plus end and the short extension as the minus end (Figure 6A).

We found that WT GFP-Kif18B localized to 46% of the 2-sided MTs, and of those MTs with motor binding events, Kif18B enriched at the distal ends of 17% of the MT plus-end extensions and only 5% of the

minus-end extensions, as would be expected for a plus end directed motor (Figure 6, A-C). A four-fold excess addition of importin α/β to the reaction resulted in increased GFP-Kif18B binding events to 73% of the MTs, $p<0.05$ (Figure 6B), suggesting that the binding of importins to Kif18B may serve as a delivery mechanism for targeting Kif18B to MTs. Furthermore, the presence of importin α/β increased the percentage of binding events at the distal MT plus-ends to 33% of the motor bound MTs, $p<0.01$ (Figure 6C). In addition to a higher percentage of MTs with motor binding events, the importins also increased the median number of binding events per MT compared to without the importins, $p<0.001$ (Figure 6D). In contrast, addition of EB1 did not increase the mean percentage of MTs with binding events, the mean percentage of bound MTs with distal plus end binding, nor the median number of binding events per MT compared to GFP-Kif18B alone (Figure 6, A-D). Examination of the minus ends of bound MTs revealed increases in distal minus-end localization compared to GFP-Kif18B alone wherein addition of the importins increased localization to 19%, $p<0.05$, and EB1 increased localization to 13%, $p<0.05$ (Figure 6C). Together, these results suggest that the presence of the importins increases the association of Kif18B to MTs, which results in a net increase in plus end localization.

Polymerization of dynamic MTs is stochastic and results in a non-Gaussian or lognormal distribution of MT lengths (Figures, 6A and S4A). To understand how importin α/β or EB1 affect the MT destabilization activity of Kif18B, we plotted the lengths of the entire seeded MTs (2-sided MT) as well as the lengths of their seeds, plus-end extensions, and minus-end extensions on a log scale to better represent their distributions (Figure 6, E-H). GFP-Kif18B did not cause a reduction in the median length of the 2-sided MTs, the seeds, plus-end extensions, or minus-end extensions compared to the GFP control. In contrast, addition of importin α/β stimulated GFP-Kif18B activity and resulted in a 2 μm reduction in the median 2-sided MT length (10.6 μm for the GFP + importin α/β control; 8.6 μm for GFP-Kif18B + importin α/β, $p<0.0001$) and a 1.5 μm reduction in the plus-end extension length (4.5 μm for the GFP + importin α/β control; 3.0 μm for GFP-Kif18B + importin α/β, $p<0.0001$) without a change in the seed or minus-end extension lengths (Figure 6, F and H). Furthermore, reactions with importin α/β addition to GFP-Kif18B resulted in numerous short MT extension fragments with Kif18B binding that could be destabilization by-products or sequestered tubulin (Figure S4A). Addition of EB1 to GFP-Kif18B did not decrease the 2-sided MT length compared to the GFP + EB1 control but resulted in a moderate decrease in plus-end extension length by 1.1 μm (4.2 μm to 3.1 μm), $p<0.05$ (Figure 6, E and G), without affecting the seed or minus-end extension lengths (Figure 6, F and H). The observation that EB1 did not significantly increase the percentage of MTs with motor binding events nor the percentage of distal plus-end MT binding, yet still reduced MT length, is consistent with the idea that the importins enhance the MT destabilization activity of Kif18B by a mechanism distinct from EB1.

Discussion

In this study we defined the critical regions of interaction between the Kif18B tail and its binding partners, the nuclear transport receptors importin α/β and EB1 and show how these interactions control Kif18B function in cells and activity *in vitro*. Our work uncovers a new mechanism by which the spatial activity of Kif18B is controlled through the RanGTP pathway. We show that the importins bind directly to the tail of Kif18B to

increase its MT association, which promotes proper plus end localization. We propose that this interaction is important for delivering Kif18B to the MTs in spindle regions outside the RanGTP gradient, which facilitates Kif18B localization to the MT plus tips at the cortex (Figure 7A). These findings suggest that the nuclear transport machinery (Ran and importins) is important to modulate spindle assembly factors in the vicinity of the chromosomes as well as distant from the chromatin, which may be a more general mechanism for modulating both the affinity and spatial distribution of MT binding proteins. Our cellular findings also support previous studies showing that disruption of Kif18B interaction with EB1 decreases its association with MT ends (Stout *et al.*, 2011b; Tanenbaum *et al.*, 2011; McHugh *et al.*, 2018), which is critical for the ability of Kif18B to control the length of astral MTs. In this study, we show for the first time that the importins and EB1 stimulate Kif18B MT destabilization activity *in vitro*. These biochemical findings suggest that the importins and EB1 regulate Kif18B MT destabilization in cells through distinct mechanisms, wherein the importins function to increase Kif18B MT binding and facilitate localization to the MT plus-end, and EB1 functions specifically at MT plus-ends for Kif18B accumulation (Figure 7B).

EB1 and Importins Cooperate to Modulate Kif18B Activity

It is well established that the Kif18B tail binds to EB1 and that this interaction is needed for MT plus-end accumulation in cells (Stout *et al.*, 2011b; Tanenbaum *et al.*, 2011; McHugh *et al.*, 2018), but how other regulatory factors govern the interaction of Kif18B with MTs is less clear. Kif18B is a plus-end directed motor that is mostly diffusive with short runs of directed motility that is mediated by a second MT binding domain in the tail (Shin *et al.*, 2015). The presence of the tail decreases the MT off-rate, increases processivity of the motor, and increases the dwell time at the MT plus-end, indicating the importance of the tail in Kif18B MT destabilization (Shin *et al.*, 2015; McHugh *et al.*, 2018). Blocking the interaction of Kif18B with EB1 using EB1 site-specific mutations prevented MT plus-end accumulation and MT length control in Kif18B knockdown cells, but these mutations in the tail had no effect on MT binding *in vitro*, indicating that EB1-mediated plus end binding in cells is strictly through EB1-Kif18B interaction. *In vitro* EB1 addition did not affect tail MT affinity, MT association of the full-length Kif18B protein to dynamic MTs, nor Kif18B MT plus-end localization; yet we did see a reduction in plus-end extension length in our dynamic MT seed assay, suggesting EB1 is promoting Kif18B activity specifically at MT plus-ends. Surprisingly, we also saw an apparent increase in distal MT minus-end localization of Kif18B in the presence of EB1 and importin α/β, which might suggest that Kif18B also functions at MT minus-ends. Consistent with this idea, a truncated Kif19A protein containing only the motor domain, neck-linker, and neck coiled coil could depolymerize MTs from the minus ends, albeit 18-fold less efficient than from the plus end (Niwa *et al.*, 2012). However, we do not favor this idea because we did not see a decrease in the minus-end extension length in the presence of EB1 or importin α/β. Another possibility for the increase in MT minus-end binding events could be that Kif18B destabilized the plus-end extension to a length shorter than the minus-end extension, which then scored as a minus-end extension in our analysis. To assess this possibility, we re-categorized the distal MT minus-end binding events of GFP-Kif18B ± EB1 or importin α/β as distal MT plus-end binding events, if the originally categorized plus-end extension length was less than 2.7 μm, which accounts for 90% of the minus-end control MT lengths. In the reactions with GFP-

Kif18B and EB1, this re-categorization increased the number of plus-end binding events to 34% compared to 20% with GFP-Kif18B alone, $p<0.05$, and reduced the minus-end binding events to 2%, like GFP-Kif18B alone (Figure S4B), suggesting that EB1 promotes Kif18B plus-end localization that in turn enhances Kif18B MT destabilization activity. Similarly, for GFP-Kif18B with importin α/β addition, this re-categorization shifted the percentage of MTs with distal plus-end localization to 44% relative to GFP-Kif18B alone, $p<0.01$, and reduced the distal MT minus-end localization to 8% compared to only 2% with GFP-Kif18B alone, $p<0.05$ (Figure S4B). Together, these observations support the idea that EB1 directly enhances Kif18B MT plus-end localization where it can act to regulate MT dynamics.

In cells, mutation of the importin α binding sites in the NLS mutant or treatment of cells with importazole disrupted Kif18B plus-end localization, suggesting importin α/β association with Kif18B promotes MT plus-end localization. In our dynamic MT seed assay, addition of importin α/β had a much more pronounced effect compared to EB1 addition in which importin α/β increased the binding of Kif18B to MTs, resulting in higher plus-end localization and greater reduced plus-end extension length. These findings agree with previous computer simulations of MT destabilizers on dynamic MTs, which showed that increasing the on-rate of a plus-end directed MT capping protein results in more motor binding at MT plus-ends and reduced MT length (Weaver *et al.*, 2011). In addition, the increased MT binding of Kif18B in the presence of importin α/β suggests that the importins favor motor association with MTs. One idea is that the Kif18B tail binds to the motor and autoinhibits the motor from binding MTs, akin to other kinesins that are autoinhibited in solution (Friedman and Vale, 1999; Imanishi *et al.*, 2006; Espeut *et al.*, 2008; Verhey and Hammond, 2009; Hammond *et al.*, 2010). We postulate that importin binding to the tail relieves this autoinhibition, allowing Kif18B to bind to MTs. Alternatively, the importins could act as a co-factor for MT association, which would be consistent with MAP7 acting to help load Kinesin-1 to MTs to modulate its activity (Ferro *et al.*, 2022). These results suggest that the importins stimulate Kif18B MT destabilization activity by increasing binding to MTs, which results in increased plus-end localization.

Our results indicate that at least two mechanisms are in play to regulate Kif18B function in cells. First, we postulate that Kif18B is loaded onto MTs in regions of the spindle outside the RanGTP gradient through its tail interaction with importin α/β, which facilitates Kif18B association with MTs and accumulation at plus ends (Figure 7A, MT loading). One possibility is that around the chromosomes where RanGTP is high, Kif18B tail interacts with the motor domain, preventing MT association (Figure 7, A and B1). Thus, outside the RanGTP gradient, importin binding could relieve this inhibition to allow the motor domain to bind MTs (Figure 7, A and B2). Kif18B is a moderately processive motor and switches between directed and diffusive motility through a tail-MT interaction that tethers it to MTs (Shin *et al.*, 2015). Interestingly, tailless versions of Kif18B are faster but less processive, and have decreased dwell times at MT plus-ends, which highlights the importance of the tail to Kif18B function (Shin *et al.*, 2015; McHugh *et al.*, 2018). A confusing observation is that our data show importin α/β inhibit Kif18B tail MT binding, yet the importins increased MT association and plus ending binding of the full-length protein. To reconcile these paradoxical results, we propose that importin α/β binding may allow for increased directed motility of Kif18B by modulating tight tail MT binding without abolishing complete

binding since the importins minimally reduced tail maximal MT binding. Consistent with this idea of the importins modulating tail MT binding, it was shown previously that Kif18B with a C-terminal GFP tag (McHugh *et al.*, 2018) has seven times higher velocities and ten times higher run lengths than N-terminally tagged Kif18B (Shin *et al.*, 2015). The authors interpreted these differences as being due to interference of the N-terminal GFP with Kif18B activity. Our findings with the importins raise the possibility that the C-terminal GFP tag may actually interfere with either tail-motor and/or tail-MT interactions. The reduced MT localization that we observed with our NLS mutant expressed in cells may be because it is stuck in an autoinhibited state that cannot be relieved by importin binding due to the NLS mutations. Alternatively, any NLS mutant protein that does associate with the MT likely does not translocate to the MT ends either because it cannot interact with the importins or because it has inherent reduced tail MT affinity. If the NLS mutant reaches MT plus-ends, it would also not be expected to accumulate because of reduced tail-MT interaction, which is necessary for plus-end retention (Su *et al.*, 2011; Shin *et al.*, 2015; McHugh *et al.*, 2018).

The second mechanism that we propose is that at the MT plus-ends in cells where EB1 is enriched as protein comets, motile Kif18B encounters EB1 bound to the MT that favors Kif18B tail-EB1 interaction, facilitating Kif18B accumulation at MT plus-ends, which in turn regulates MT dynamics (Figure 7A, Competition for end-binding). Our biochemical data shows that the importins can compete with EB1 for binding to the Kif18B tail, but it may be that at the plus-ends of MTs in cells where EB1 is enriched and bound to MTs, EB1 can out compete the importins for binding to the Kif18B tail to promote Kif18B plus-end accumulation (Figure 7, A and B4). Cellular work clearly demonstrates that Kif18B tail interaction with EB1 is essential for Kif18B localization to astral MT plus-ends (Stout *et al.*, 2011b, this study; McHugh *et al.*, 2018). Once Kif18B is near the MT end, the polymerizing plus end may have a more favorable binding conformation that stimulates Kif18B MT destabilization activity (Figure 7B5). For example, the Kip3 motor domain is proposed to undergo a binding switch at the plus tips that stimulates MT depolymerization through suppressed ATPase activity and strong interaction of the motor domain with the curved growing protofilaments (Arellano-Santoyo *et al.*, 2017). Similarly, based on structural studies of the Kif19A motor domain bound to MTs, Kif19A may also undergo a nucleotide-dependent conformational change at MT plus-ends that stabilizes curved protofilaments and induces depolymerization (Niwa *et al.*, 2012). In addition, mathematical modeling indicates that MT destabilization by Kinesin-8s may be a function of the concentration of the protein at the plus end as well as the speed at which it reaches the end (Reese *et al.*, 2011). Thus, importin α/β may function to increase the rate of Kif18B reaching plus ends and EB1 coordinates the concentration for efficient MT destabilization.

The RanGTP Gradient Spatially Controls MT Binding Affinity of Motor Proteins

One important outcome of our studies is that the interaction of the Kif18B tail with the importins is likely critical for the spatial regulation of motor function. In monopolar spindles, while the NLS mutant localization is diminished on the MTs, sufficient Kif18B reaches the ends to destabilize the MTs and control aster size. While the NLS mutant is indistinguishable from wild type to control astral MT length, it is defective in inducing spindle bipolarization when overexpressed. This suggests that either the inability to properly enrich on MT ends of cortical MTs is critical or that the spatial control of Kif18B near the cortex is critical to set up pulling forces on

astral MTs that are important in spindle bipolarity. These findings support previous data showing that Kif18B is important in bipolar spindle assembly in Eg5 independent cells (van Heesbeen *et al.*, 2017).

The RanGTP system is generally utilized to govern nuclear/cytoplasmic transport. In mitosis, Ran plays a key role in the spatial control of spindle assembly factors around chromosomes (Kalab and Heald, 2008) and regulates factors at kinetochores and spindle poles. Previous findings suggest that RanGTP can control protein localization outside of the spindle. For example, it has been shown that RanGTP controls the localization of NuMA-LGN at the cortex (Kiyomitsu and Cheeseman, 2012), wherein LGN localization is reduced in areas of the cortex within 2 μm of the chromatin. While we have not observed Kif18B localization to the cortex, a recent study in keratinocytes showed that Kif18B does localize to the cortex where it co-localized with NuMA (Moreci and Lechler, 2021). Loss of either Kif18B or LGN lead to defects in spindle position that are presumably linked to disruptions in MT-cortical interactions (Blumer *et al.*, 2006; Kiyomitsu and Cheeseman, 2012; Zheng *et al.*, 2013). It is interesting to note that our Kif18B NLS mutant was able to rescue astral MT length in monopolar spindles, which could be due to the dispersed organization of the chromosomes in the monopolar spindle that position them sufficiently close to the cortex to not block that interaction. In addition, it was shown that importazole addition disrupted spindle centering when added to cells (Soderholm *et al.*, 2011), but there was no indication of the Ran target that was important in this process. Our findings that importazole directly disrupts Kif18B localization implicates Kif18B as a Ran-regulated target acting at the cortex. Together, these studies also support the idea that RanGTP may act as a global control center to modulate spatial regulation during mitosis, not only around chromosomes but throughout the cell.

Another emerging theme from our studies is that importin α/β may be a major mechanism to control the affinity of MT binding. Spindle assembly factors regulated by Ran include the molecular motors XCTK2 (Ems-McClung *et al.*, 2004; Ems-McClung *et al.*, 2020) and Kif18B (this study) as well as microtubule binding proteins NuMA (Wiese *et al.*, 2001) and TPX2 (Gruss *et al.*, 2001; Schatz *et al.*, 2003a; Schatz *et al.*, 2003b). For the molecular motor proteins, each of these motors has a second microtubule binding site in the tail that is used for either cross-linking or for motor processivity. Importin α/β binding was competitive with MT binding, and for the Kinesin-14 XCKT2, it controlled the affinity of MT binding (Ems-McClung *et al.*, 2004). One possibility is that MT binding sites are often basic, similar to the canonical bipartite NLS (Conti *et al.*, 1998; Kosugi *et al.*, 2009), and so coincidentally these sites are similar. A more interesting possibility is that in proteins with an NLS, the NLS region may serve as a MT binding domain with a distinct binding site on the MT itself. Structural studies are beginning to reveal that different motors and MAPs bind to distinct regions of the MT surface (Nogales and Zhang, 2016) and that these unique binding regions may help explain how multiple MAPs can be bound to a MT. This binding geometry could be important to load the motors onto the MT. Alternatively, tail MT binding may be important to position the motor head either to a different tubulin dimer on the same MT or, in the case of cross-linking motors, to another MT. Future structural studies identifying how the NLS-containing motor tails bind MTs will be important to dissect this idea.

Materials and Methods

Cloning and site-directed mutagenesis

To express His_6-EB1-CyPet, full length human EB1 was amplified by PCR from pET30a-EB1 ((Stout *et al.*, 2011), a gift from Jennifer Tirnauer) using the primers in Table S1. The resulting PCR product was cloned into the *Xba*I/*Xho*I sites of pRSETB-CyPet (Ems-McClung *et al.*, 2020) to create pRSETB-EB1-CyPet. For expression and purification of the C-terminal tail proteins of human Kif18B (Kif18B) fused to YPet, we generated plasmids with an N-terminal YPet tag and a C-terminal His_6 tag in two steps. We first generated plasmids encoding YPet fused to the full length Kif18B tail (aa 605-828) amplified from pDEST15-Kif18B(CT605-828) and the far C-terminus (aa 708-828) amplified from pDEST15-Kif18B(CT708-828) (Stout *et al.*, 2011) using the primers in Table S1. The resulting PCR fragments were cloned into pRSETB-YPet (Ems-McClung *et al.*, 2020) digested with *Sac*II/*Pst*I creating pRSETB-YPet-Kif18B(605-828) and pRSETB-YPet-Kif18B(708-828). To generate plasmids with a C-terminal His_6 tag, DNAs encoding YPet-Kif18B(605-828) and YPet-Kif18B(708-828) were PCR amplified from the pRSETB-YPet constructs using primers in Table S1 and cloned into the pET24b(+) *Bam*HI/*Sal*I sites to generate pET24b(+)-YPet-Kif18B(605-828) and pET24b(+)-YPet-Kif18B(708-828), respectively. To generate pET24b(+)-YPet-Kif18B(605-707), DNA encoding YPet-Kif18B(605-707) was PCR amplified from pRSETB-YPet-Kif18B(605-828) using the primers in Table S1 and cloned into the pET24b(+) *Bam*HI/*Sal*I sites.

Two putative nuclear localization signal (NLS) sequences in the tail of Kif18B were predicted using the web-based predication program cNLS Mapper (http://nls-mapper.iab.keio.ac.jp/cgi-bin/NLS_Mapper_form.cgi). The putative non-canonical bipartite sequence (NLS1) was further evaluated using guidelines described by (Kosugi *et al.*, 2009) to determine the residues critical for importin α binding. The codons encoding the NLS1 basic residues, indicated in bold, ^{639}**KKR**RRPSALEADSPMAP**KR**^{657} were mutated sequentially to alanine with the NLS1a and NLS1b primer sets listed in Table S2 using the QuikChange site-directed mutagenesis system (Agilent, San Diego, CA) to create pET24b(+)-YPet-Kif18B(605-828)-NLS1. Likewise for the second putative NLS (NLS2), the codons encoding the basic residues of the putative monopartite sequence ^{795}**KKKR**^{798} were mutated to alanine with the primers in Table S2 to create pET24b(+)-YPet-Ki18B(605-828)-NLS1/2 and pET24b(+)-YPet-Kif18B(708-828)-NLS2, respectively. To generate pET24b(+)-YPet-Kif18B(605-707)-NLS1 containing only the NLS1 mutations, DNA was amplified from pET24b(+)-YPet-Kif18B(605-828)-NLS1 and cloned into the *Bam*HI/*Sal*I restriction sites of pET24b(+).

To identify the EB1 binding sites in the tail of Kif18B, the codons encoding the last two residues, indicated in bold, of the three previously reported EB1 binding sites (Tanenbaum *et al.*, 2011), ^{665}SF**LP**^{668} (E1), ^{786}SS**LP**^{789} (E2), and ^{812}AR**LP**^{815} (E3), were mutated to asparagine (Honnappa *et al.*, 2009) using the QuikChange site-directed mutagenesis system and the primers listed in Table S2. Double EB1 mutants were generated by sequential site-directed mutagenesis. All constructs were verified by sequencing.

Protein expression and purification

For the expression of His_6-EB1-CyPet, His_6-EB1 (Stout *et al.*, 2011), His_6-importin α-CyPet (Ems-McClung *et al.*, 2020), His_6-importin β, and importin α-His_6 (Ems-McClung *et al.*, 2004) recombinant proteins, plasmids

were transformed into BL21(DE3)pLysS bacteria and induced with 0.1 mM isopropyl β-D-1-thiogalactopyranoside (IPTG) at 16°C for 24 h. For the expression of YPet-Kif18B-His_6 recombinant proteins, plasmids were transformed into SHuffle T7 Express LysY bacteria (NEB Cat# C3030J) and induced with 0.4 mM of IPTG at 16ºC for 24h. Cells were pelleted, frozen in liquid nitrogen, and stored at -80ºC. For protein purification using NiNTA agarose (Qiagen), cells were lysed in 50 mM phosphate buffer, pH 8.0, 300 mM NaCl, 10 mM imidazole, 0.1% Tween-20, 1 mM PMSF,1 mM benzamidine, 0.5 mg/ml lysozyme and sonicated four to six times using a Branson Sonifer at 20% output. Immediately after sonication, the salt concentration was increased to 500 mM by adding NaCl, and β-mercaptoethanol (β-ME) added to a final concentration of 5 mM. The lysate was clarified at 18,000 rpm for 20 min at 4°C in a Beckman JA25.5 rotor. The supernatant was added to NiNTA agarose equilibrated with Column Buffer (50 mM phosphate pH 8.0, 500 mM NaCl, 0.1% Tween-20, 10 mM imidazole) in a 50 ml falcon tube and incubated at 4°C for 1 h with rotation. The clarified lysate-bead mixture was centrifuged in a clinical centrifuge for 4 min at setting 4 to pellet the beads, which contained the bound protein of interest. After discarding the supernatant, the agarose beads were washed twice in 10 column volumes (CV) of Column Buffer containing 1 mM PMSF, 1 mM benzamidine, 5 mM β-ME for 10 min with rotation. Ten CV of Column Wash Buffer (50 mM phosphate buffer, pH 6.0, 500 mM NaCl, 5 mM β-ME, 0.1 mM PMSF) was added to the pelleted beads and loaded into a disposable column at 4°C. Once the Column Wash Buffer was drained, the bound protein was eluted with 10 CV of Elution Buffer (50 mM phosphate buffer, pH 7.2, 500 mM NaCl, 400 mM imidazole, 5 mM β-ME) at 4°C in 1 mL aliquots. For the purification of YPet-Kif18B-His_6 tail proteins, 1 µg/ml leupeptin, 1 µg/ml pepstatin, 1 µg/ml chymostatin, and 1 mM PMSF were added to all the purification buffers. For His_6-EB1-CyPet, His_6-importin α-CyPet, His_6-S-importin β, importin α-His_6, and His_6-EB1, eluted fractions containing the highest amounts of protein were dialyzed into XB dialysis buffer (10 mM HEPES, pH 7.2, 100 mM KCl, 25 mM NaCl, 50 mM sucrose, 0.1 mM EDTA, 0.1 mM EGTA) overnight at 4ºC. The proteins were further dialyzed for an additional 3 hours the next morning. YPet-Kif18B-His_6 proteins were similarly dialyzed into XB500 (10 mM HEPES, pH 7.2, 500 mM KCl, 50 mM sucrose, 0.1 mM EDTA, 0.1 mM EGTA). The dialyzed proteins were snap-frozen in liquid nitrogen in single use aliquots and stored at -80ºC.

Förster resonance energy transfer (FRET) of Kif18 interaction with importin α/β or EB1

The interactions between human Kif18B and human importin α/β or EB1 were reconstituted *in vitro* by using the FRET biosensors, His_6-importin α-CyPet, His_6-EB1-CyPet, and YPet-Kif18B-His_6 tail domains in solution as described previously (Ems-McClung and Walczak, 2020). To determine saturable binding, 100 nM of His_6-importin α-CyPet together with 400 nM S-His_6-importin β or 100 nM of His_6-EB1-CyPet were mixed with 100 nM-1.0 µM YPet tagged Kif18B tail fragments in Reaction Buffer (10 mM HEPES pH 7.2, 55 mM ionic strength, 50 mM sucrose, 0.1 mM EDTA, 0.1 mM EGTA, 0.1 mg/ml casein). Where indicated, RanQ69L was added to a final concentration of 10 µM to the YPet-Kif18B tail + importin α-CyPet/importin β reactions after an initial FRET measurement, incubated for 10 min at RT, and FRET measured again (Ems-McClung and Walczak, 2020). To achieve a final ionic strength of 55 mM, XB dialysis buffer was added to the reactions accounting for the KCl and NaCl contributed by the different proteins. A 50 µl aliquot of each reaction mix was

transferred to a Costar #3964 96-well ½ area black plate and incubated at room temperature for 10 min before performing a spectral scan in a Synergy H1 plate reader (Bio-Tek). The spectral scan was performed by exciting His_6-importin α-CyPet or His_6-EB1-CyPet at 405 nm and recording the emission from 440 to 600 nm with 5 nm steps (Ems-McClung and Walczak, 2020). The recorded data was processed in Excel by subtracting the background YPet emission in control reactions without CyPet protein from YPet emission in the presence of CyPet protein, and the net emission was then normalized to the CyPet emission at 460 nm to obtain FRET ratios at 530 nm. Graphs of the FRET ratio means ± SEM were plotted relative to the different molar ratios of importin α-CyPet and hEB1-CyPet in Prism (GraphPad). For competition assays, a premix comprising 100 nM His_6-importin α-CyPet, 400 nM of His_6-importin β and 400 nM His_6-EB1 or 100 nM His_6-hEB1-CyPet, 400 nM of importin α-His_6, and His_6-importin β were prepared and then added to 800 nM of YPet-Kif18B-His_6 tail fragments in Reaction Buffer and processed for FRET as described.

Full-length human Kif18B N-terminally tagged with enhanced green fluorescent protein (EGFP), GFP-Kif18B, was expressed in Sf-9 insect cells at an MOI of 2 from baculovirus generated from pFB-EGFP-Kif18B-siRNA^R using Gateway technology with pENTR-EGFP-Kif18B-siRNA^R (see Lentivirus Production below) and pFastBac1-DEST plasmids. pFastBac1-DEST was generated by amplifying the destination cassette (ccdB and chloramphenicol resistance genes) from pDEST^{TM}15 (ThermoFisher) with flanking attR1/R2 sites (Table S1) and inserting them into the SacI/KpnI sites of pFastBac1. Expressed GFP-Kif18B was purified by cation exchange chromatography using a 1 mL HiTrap SP column and by size exclusion using a Superose 6 HR 10/30 column in 20 mM Pipes pH 6.8, 300 mM KCl, 1 mM $MgCl_2$, 1 mM EGTA, 0.1 mM EDTA, 1 mM DTT, 0.1 mM ATP, 0.1 µg/mL LPC. Solid sucrose was added to 10%, aliquoted, frozen in liquid nitrogen, and stored at -80°C (Ems-McClung *et al.*, 2004).

Lentivirus production

To produce lentivirus for expression of human Kif18B N-terminally tagged with EGFP, GFP-Kif18B, containing the NLS and EBBD mutations in mammalian cells, pLOVE constructs containing siRNA resistant (siRNA^R) Kif18B were made using Gateway technology. To generate pENTR-EGFP-Kif18B-siRNA^R, the EGFP-Kif18B sequence from pEGFP-DEST-Kif18B (Stout *et al.*, 2011) was amplified using the primers in Table S1, cloned into pENTR/D-TOPO (Invitrogen), and silent mutations introduced to confer resistance to siRNA of Kif18B by QuikChange site-directed mutagenesis using the primers in Table S2. Subsequent rounds of site-directed mutagenesis were used to create pENTR-EGFP-Kif18B-siRNA^R-NLS1/2 with the pENTR-Kif18B-NLS1a, pENTR-Kif18B-NLS1b, and pENTR-Kif18B-NLS2 forward and reverse primers and pENTR-EGFP-Kif18B-siRNA^R-EBBD1/3 with the pENTR-Kif18B-EBBD1 and pENTR-Kif18B-EBBD3 forward and reverse primers in Table S2. Entry vectors were recombined into the pLOVE destination vector (Addgene #15948) using Gateway technology. All clones were verified by sequencing.

HEK293T cells were maintained in Gibco™ DMEM, High Glucose supplemented with GlutaMAX™ and pyruvate (Thermofisher), and 10% fetal bovine serum (Corning) at 37°C and 5% CO_2 in a humidified incubator. Lentiviruses were produced by co-transfecting 1 µmol of pLOVE-EGFP-Kif18B-siRNA^R, pLOVE-EGFP-Kif18B-

siRNA^R-NLS1/2, or pLOVE-EGFP-Kif18B-siRNA^R-EBBD plasmids with 1 μmol each of the packaging plasmids dRT-pMDLg/pRRE (Addgene #60488), pRSV-Rev (Addgene #12253), and VSV-G envelope expressing plasmid, pMD2.G (Addgene #12259) into HEK293T cells plated at 1.5 x 10^5 cells/ml in T-25 flasks using Lipofectamine 3000 (Thermo Fisher). Media was changed 6-8 h post-transfection, and media containing virus was collected at 24 h and 48 h post-transfection, filtered, and stored at -80°C in single use aliquots. Functional titers of these viruses were determined post 48h of viral transduction as described in Addgene: Fluorescence Titering Assay using 96-well clear bottom plates (Corning #3603).

Kif18B siRNA knockdown and EGFP-Kif18B-siRNA^R lentiviral expression

HeLa cells were maintained in Gibco™ DMEM, High Glucose supplemented with GlutaMAX™, pyruvate, and 10% fetal bovine serum at 37°C and 5% CO_2 in a humidified incubator. For Kif18B knockdown and/or EGFP-Kif18B-siRNA^R lentiviral expression assays, 5 x10^4 HeLa cells were seeded on coverslips in 6-well plates. After 24 h, cells were transfected with 40 nM RNAi oligonucleotides using Lipofectamine RNAiMax (Invitrogen) according to the manufacturer's instructions. The following siRNAs (Dharmacon) were used: Neg2 (5'-UGGUUUACAUGUUGUGUGA-3') or Kif18B siRNAi (5'- CAGUUUCCAUGAAUGCAUUUU-3') (Stout *et al.*, 2011). After 24 h, the transfection media was removed, and the HeLa cells were transduced with lentivirus particles with a MOI of 0.5 in presence of 10 μg/ml of polybrene in complete media without antibiotics. To form monopolar spindles, lentivirus media was removed 36 h post infection and replaced with fresh media containing 100 μM Monastrol and incubated for 12 h prior to fixation.

Western blot

To probe Kif18B depletion by Western blot, 120,000 HeLa cells were seeded per well in a 6 -well plate and after ~24 h, cells were transfected with control siRNA (Neg2) or Kif18B siRNA. Cells were released from transfection after 24 h, allowed to grow for 6 h and then synchronized by treating with 6.0 μM Cdk1 inhibitor, RO3306 (Sigma, #SML0569) for 16 h followed by 100 μM Monastrol treatment for 4 h. Cells were trypsinized and resuspended in 1X PBS containing 100 μM Monastrol. 50,000 and 25,000 cells in 2X sample buffer were loaded on to 10% SDS-PAGE, transferred to nitrocellulose membrane (Biotrace, #66485) for Western blot analysis. The blot was blocked in 5% non-fat dry milk in TBS-T (20 mM Tris, pH7.5, 150 mM NaCl with 0.1% Tween-20), probed with affinity purified rabbit anti-Kif18B (2.5 μg/ml) in Ab-Dil-T ((20 mM Tris, pH 7.5, 150 mM NaCl, 2% BSA, 0.1% Tween-20) as a primary antibody. Donkey anti-rabbit IgG HRP (Thermo Fisher Scientific, #45000682) (1:10,000) in 5% nonfat dry milk in TBS-T was used as a secondary antibody. Blots were incubated with SuperSignal West Pico Chemiluminescent Substrate (ThermoFisher Scientific, Rockford, IL) and exposed to Amersham Hyperfilm ELC (GE Healthcare). The film was developed using SRX-101A, Medical Film Processor (Konica Minolta Medical and Graphic, Inc).

Importazole treatment

40,000 cells were seeded per well in a six well plate. After 72h, these cells were treated with 100 μM Monastrol for 12h followed by a treatment with either DMSO or 20 μM Importazole (Selleck Chemicals Houston, TX, #S8446) in presence of 100 μM Monastrol for 1h before fixation and staining.

Immunofluorescence

For immunofluorescence, cells were rinsed in phosphate-buffered saline (12 mM phosphate, 137 mM NaCl, 3 mM KCl, pH 7.4) and then fixed in -20°C MeOH for 10 min. Cells were blocked in Abdil-Tx (20 mM Tris, 150 mM NaCl, pH 7.5 (TBS), 0.1% Triton X-100, 2% bovine serum albumin, 0.1% sodium azide) for 30 min at room temperature (RT). Cells were stained with rabbit anti-GFP (2.5 μg/ml) and mouse DM1α (1:500, Sigma-Aldrich T6199), rabbit anti-Kif18B serum (1:2000) or mouse anti-EB1 (0.5 μg/ml, BD Transduction Laboratories) primary antibodies for 30 min at RT, washed with TBS-Tx (TBS with 0.1% Triton X-100), and then stained with Alexa Fluor 488 donkey anti-rabbit (2 μg/ml, Invitrogen #A21207) and Alexa Fluor 594 goat anti-mouse (2 μg/ml, Invitrogen #A10239) secondary antibodies for 30 min at RT. DNA was stained with 10 μg/ml Hoechst for 5 min (Sigma-Aldrich) after being washed with TBS-Tx and then mounted in Prolong Diamond (Invitrogen #P36961).

For the analysis of bipolar spindles in Monastrol-treated cells (Figure 6), 4 $x10^3$ HeLa cells were seeded in a 96-well clear bottom plate (Corning #3603). After 24 h, cells were transfected with 40 nM RNAi oligonucleotides using Lipofectamine RNAiMax as above. After 24 h, the transfection media was removed, and the cells were infected with lentivirus particles in complete medium containing 10 μg/ml polybrene. To form monopolar spindles, lentivirus media was removed 32 h post infection and replaced with fresh media containing 100 μM Monastrol and incubated overnight prior to fixation. Cells were fixed in -20°C MeOH with 1% formaldehyde for 5 min, blocked, and stained with mouse DM1α (1:500) for primary antibodies as described above. Alexa Fluor 594 goat anti-mouse (2 μg/ml) was used as a secondary antibody. DNA was stained with 10 μg/ml Hoechst, and then the plates were stored in phosphate-buffered saline (PBS; 137 mM NaCl, 2.7 mM KCl, 10 mM Na_2HPO_4, 1.8 mM KH_2PO_4, pH 7.2) before imaging.

Microscopy

For analysis of aster area, images were collected with a 40X 1.0 PlanApo objective or with a 60X 1.42 PlanApo objective for analysis of GFP localization on a Nikon 90i equipped with a CoolSnap HQ CCD camera (Photometrics) and controlled by Metamorph (Molecular Devices). Image stacks were collected through the entire cell volume at 0.4 μm and 0.2 mm steps for 40X and 60X objectives respectively. Each individual channel was imaged with equivalent exposure times across all samples. For the analysis of Kif18B localization on monopolar spindles, cells transduced with GFP-Kif18B WT or NLS mutant lentiviruses or Importazole treated cells were imaged using the OMX SR 3D-SIM Super-Resolution system (GE DeltaVision) controlled by AquireSR software. Images were captured at 0.125 μm step size with an PlanApo N 60X 1.42 NA oil PSF objective, using 1.518 immersion oil. The 405 nm wavelength images were acquired at 1% laser strength, 488 nm wavelength images at 3% laser strength, 564 nm wavelength images at 4% laser strength with equivalent

exposure times. Images were processed using softWoRx (Applied Precision, Inc.) and Imaris 3D imaging software (Bitplane Inc.).

Image analysis and quantification

Composite images were generated and processed identically using FIJI. Aster areas were measured in FIJI by manually drawing a circle around each MT aster in the red channel and then transferring that ROI to the green channel. To determine the range of GFP fluorescence for analysis, cells with either control or Kif18B knockdown were mock-transduced and then stained with anti-GFP antibodies as described above. The average fluorescence in the green channel in these cells was considered background and was used to determine the lower threshold for GFP fluorescence. To determine the upper level of the GFP fluorescence that could be used to assess the level of rescue of our WT and mutant constructs, we systematically tested bins of GFP fluorescence of cells with knockdown of Kif18B that were rescued with WT GFP-Kif18B lentivirus expression and used the broadest bin size that resulted in full rescue of the knockdown phenotype, which corresponded to a range of 40-2000 arbitrary units (au).

For analysis of the percentage of bipolar spindles and GFP expression levels in cells with overexpression of lentiviral GFP-Kif18B proteins, images were collected using a 20X 0.45 Olympus Plan Fluorite objective on a Lionheart FX automated microscope (BioTek). A semi-automated analysis pipeline was created using the Gen5 Image Prime software (BioTek) to measure the area of monopolar spindles and the intensity of the GFP signal. Briefly, primary masks for mitotic cells were defined by DAPI fluorescence above 50,000 au with a secondary mask of the TexasRed or the GFP channel extending up to 6 μm out from the primary mask with a threshold of 9,000 au or 10,000 au, respectively. Monopolar spindles were defined as having a length/width ratio of less than or equal to 1.25 and an area between 50-300 μm^2. GFP-Kif18B expressing cells were defined as having a GFP intensity greater than 5 $x10^7$ au. The percentage of bipolar spindles were measured by counting 100 mitotic figures and scoring the number of monopolar and bipolar spindles from three independent experiments.

Fluorescence values and aster areas were exported to Excel (Microsoft), plotted in Prism 9 (GraphPad Software), and graphs assembled in Illustrator (Adobe). Statistical analyses were performed using Prism 9. To determine if the data came from a normal distribution, a D'Agostino-Pearson omnibus normality test was performed, and a $p < 0.05$ was considered as a non-normal distribution. For comparisons of non-normally distributed GFP fluorescence and aster area, one-way analysis of variance (ANOVA) followed by a Kruskal-Wallis tests with Dunn's multiple comparisons tests were used. Fluorescence values and aster areas were plotted with the median ± interquartile range. The mean percentages of bipolar cells were plotted ± SEM. Unpaired *t*-tests were used to determine differences between the means. A $p < 0.05$ was considered significant for all tests.

Microtubule Binding and Dynamic MT Seed Assays

The interaction between Kif18B tail and MTs was measured by co-sedimentation. Doubly stabilized MTs were polymerized by incubating 5 μM tubulin with 0.5 mM GMPCPP (Jena BioScience, #NU-405L) for 20 min

at 37°C, adding paclitaxel to a final concentration of 10 μM and incubating for an additional 10 min at 37°C. MTs were pelleted at 45,000 rpm in a Beckman TLA100 rotor and then resuspended in BD Buffer (80 mM K-Pipes, pH 6.8; 1 mM $MgCl_2$; 1 mM EGTA; 1 mM DTT) + 50 mM KCl containing 10 μM paclitaxel. The MT concentration was determined using a molar extinction coefficient of 115,000 $M^{-1}cm^{-1}$ and adjusted to 10 μM with BD + 50 mM KCl. For binding reactions, 250 nM YPet-Kif18(605-828) WT or mutant derivatives were combined with 0 to 5 μM MTs, incubated for 15 min at RT and then sedimented at 45,000 rpm in a TLA 100 rotor at 25°C. The supernatant was removed to a fresh tube, and the pellet was resuspended in an equivalent volume of BD + 50 mM KCl. A 20 μl aliquot of the corresponding supernatant and pellet fractions were transferred to a Corning 384 well plate, and the fluorescence of YPet was measured with 500 nm excitation/530 nm emission on a BioTek Synergy plate reader. For competition experiments, a premix solution of 250 nM YPet-Kif18(605-828) was incubated with 500 nM importin α-His_6, and S- His_6-importin β for 5 min before adding to the MT mixture. For competition with EB1, the premix solution contained 250 nM YPet-Kif18B(605-828) and 1 mM S-His-EB1. All data was corrected for the amount of YPet-Kif18B tail that pelleted in the absence of MTs and normalized to represent fractional binding in micromolar protein bound. The average protein bound at each MT concentration were plotted as the mean ± SEM in Prism and fit with to the quadratic equation (Hertzer *et al.*, 2006).

Dynamic MT seed assays were performed by polymerizing GMPCPP stabilized Cy5-MT seeds from 4 μM HiLyte 647 tubulin (Cytoskeleton, #TL670M) in BD buffer + 0.5 mM GMPCPP at 37°C for 1 hour. Seeds were added 1:10 for final concentrations of 75 nM GFP protein ± 300 nM importin α/β or 300 nM EB1, 6 μM 17% X-rhodamine tubulin, 50 mM KCl, 2 mM ATP, 1 mM GTP in BD buffer, and incubated at 37°C for 20 min. Reactions were fixed with 40 μL of 1% glutaraldehyde/BD buffer for 3 min and diluted with 800 μL BRB80 (BD buffer without 1 mM DTT). Fixed and diluted samples were added to spin down tubes containing a removable chock, coverslip, and 5 mL BRB80 underlaid with 10% glycerol, BRB80. The spin down tubes were centrifuged for 45 min at 12,000 rpm in a JS13.1 Beckman rotor at 20°C. The coverslips were removed, immunostained with 3 μg/mL anti-GFP antibody and 2 μg/mL Alexa488 donkey anti-rabbit IgG, mounted in ProLong™ Diamond, cured for 24 h, and sealed with nail polish. Widefield FITC, TRITC, and Cy5 fluorescence images were taken on a Nikon A1 microscope equipped with a PlanApo VC 60x NA1.4 DIC NS objective and ORCA-Flash4.0 Hamamatsu camera controlled by Nikon Elements in the Light Microscopy Imaging Center at IU – Bloomington. Each image was taken at identical exposure times for each of the three channels, scaled identically in FIJI, and assembled in Adobe Illustrator.

A graphical user interface (GUI) was developed in MATLAB for interactive identification of MT seeds, extensions, and motors from three images taken with different fluorescence filter sets. MT polymer segmentation and identification was accomplished using a Hessian ridge algorithm (Steger, 1998) to identify contiguous fluorescent structures followed by a Dijkstra minimum path algorithm (Dimas, 2022) for tracing continuous points that minimize curvature and gaps. Parameters for Gaussian filters, maximum gap size, distance between seed and extension, and allowed curvature were set by the user. Motors were identified using a difference of Gaussian filtered images and a user-set threshold with user defined minimum distance to MT seed or extension. A MT binding event at the plus or minus end was considered when the motor binding

event was within three pixels or 0.3 μm from the MT end. A user driven interface allowed editing of all segmented data points overlain on to original images for verification. Results from each image were output to Excel files where they were compiled and then imported into Prism 9 for graphing and statistical analysis. In addition, output figures were generated for each image that displayed the MTs from each MT class (seed only, seed with two extensions (2-sided), seed with one extension (1-sided), and extension only) with the corresponding positioned motor binding events as identified and as linearized representations of polymer. A second MATLAB GUI was developed to compile the data from each experimental condition from independent experiments into single output Excel files and linear representations of seed, extension, and motor position. Data presented is from three independent experiments.

The percentage of MTs bound with GFP-Kif18B motor ± a four-fold excess of importins or EB1 was determined by dividing the number of 2-sided MTs that had at least one motor binding event by the total number of 2-sided MTs in that condition for each experiment, averaged, and graphed as the mean ± SEM. An unpaired Student's *t*-test was used to determine significant differences from GFP-Kif18B alone. The percentage of MTs with motor binding events at the distal plus or minus ends of the 2-sided MTs in each condition was determined by dividing the number of events at either end by the number of bound MTs, averaged, and graphed as the mean ± SEM. The criteria for determining whether a minus end with a motor binding event might be a short plus end, was considered when the plus end length was shorter than 90% of control GFP minus end length or 2.7 um. A multiple unpaired *t*-test was used to determine significance compared to GFP-Kif18B alone. The number of motor binding events per MT was plotted for each condition with the median ± interquartile range. The distribution of binding events was lognormal based on the Normality and Lognormality Test in GraphPad Prism 9. ANOVAs using the Kruskal-Wallis test with Dunn's multiple comparisons were performed for significance from WT GFP-Kif18B alone. MT lengths of the 2-sided MTs, the seeds, and the minus and plus end extensions had non-normal distributions as indicated by the Normality and Lognormality Tests in Prism. To best visualize these distributions, the lengths were graphed on a log scale with the median ± interquartile range. Significant differences in their median lengths were determined using the Kruskal-Wallis test with Dunn's multiple comparisons test. Significance was considered when $p < 0.05$ for statistical tests.

Acknowledgements

This work was supported by NIH R35GM122482 to CEW, NSF MCB2128166 to CEW, and NSF MCB1615907 to SLS. Support for the OMX 3D-SIM microscope was provided by NIH S10 OD024988-01. We thank Anjaly Prasannajith for help in making the Kif18B lentiviral constructs, and Puck Ohi and Jordon Winn for comments on the manuscript. We are indebted to Jim Powers in the IU-Light Microscopy Imaging Center for his assistance with the OMX imaging and IMARIS reconstructions. The IUB-LMIC is supported in part by the Office of the Vice Provost for Research.

References

Arellano-Santoyo, H., Geyer, E.A., Stokasimov, E., Chen, G.Y., Su, X., Hancock, W., Rice, L.M., and Pellman, D. (2017). A Tubulin Binding Switch Underlies Kip3/Kinesin-8 Depolymerase Activity. Dev Cell *42*, 37-51 e38.

Blumer, J.B., Kuriyama, R., Gettys, T.W., and Lanier, S.M. (2006). The G-protein regulatory (GPR) motif-containing Leu-Gly-Asn-enriched protein (LGN) and Gialpha3 influence cortical positioning of the mitotic spindle poles at metaphase in symmetrically dividing mammalian cells. European J Cell Biol. *85*, 1233-1240.

Caudron, M., Bunt, G., Bastiaens, P., and Karsenti, E. (2005). Spatial coordination of spindle assembly by chromosome-mediated signaling gradients. Science. *309*, 1373-1376.

Conti, E., Uy, M., Leighton, L., Blobel, G., and Kuriyan, J. (1998). Crystallographic analysis of the recognition of a nuclear localization signal by the nuclear import factor karyopherin alpha. Cell *94*, 193-204.

Desai, A., Verma, S., Mitchison, T.J., and Walczak, C.E. (1999). Kin I kinesins are microtubule-destabilizing enzymes. Cell *96*, 69-78.

Dimas, A. (2022). Dijkstra Algorithm, https://www.mathworks.com/matlabcentral/fileexchange/36140-dijkstra-algorithm MATLAB Central File Exchange.

Du, Y., English, C.A., and Ohi, R. (2010). The kinesin-8 Kif18A dampens microtubule plus-end dynamics. Curr Biol *20*, 374-380.

Ems-McClung, S.C., Emch, M., Zhang, S., Mahnoor, S., Weaver, L.N., and Walczak, C.E. (2020). RanGTP induces an effector gradient of XCTK2 and importin alpha/beta for spindle microtubule cross-linking. J Cell Biol *219*, 10.1083/jcb.201906045.

Ems-McClung, S.C., and Walczak, C.E. (2020). In vitro FRET- and fluorescence-based assays to study protein conformation and protein-protein interactions in mitosis. Methods in Mol Biol *2101*, 93-122.

Ems-McClung, S.C., Zheng, Y., and Walczak, C.E. (2004). Importin alpha/beta and Ran-GTP regulate XCTK2 microtubule binding through a bipartite nuclear localization signal. Mol Biol Cell *15*, 46-57.

Espeut, J., Gaussen, A., Bieling, P., Morin, V., Prieto, S., Fesquet, D., Surrey, T., and Abrieu, A. (2008). Phosphorylation relieves autoinhibition of the kinetochore motor Cenp-E. Mol Cell *29*, 637-643.

Ferro, L.S., Fang, Q., Eshun-Wilson, L., Fernandes, J., Jack, A., Farrell, D.P., Golcuk, M., Huijben, T., Costa, K., Gur, M., DiMaio, F., Nogales, E., and Yildiz, A. (2022). Structural and functional insight into regulation of kinesin-1 by microtubule-associated protein MAP7. Science. *375*, 326-331.

Friedman, D.S., and Vale, R.D. (1999). Single-molecule analysis of kinesin motility reveals regulation by the cargo-binding tail domain. Nat Cell Biol *1*, 293-297.

Gruss, O.J., Carazo-Salas, R.E., Schatz, C.A., Guarguaglini, G., Kast, J., Wilm, M., Le Bot, N., Vernos, I., Karsenti, E., and Mattaj, I.W. (2001). Ran induces spindle assembly by reversing the inhibitory effect of importin a on TPX2 activity. Cell *104*, 83-93.

Gupta, M.L., Jr., Carvalho, P., Roof, D.M., and Pellman, D. (2006). Plus end-specific depolymerase activity of Kip3, a kinesin-8 protein, explains its role in positioning the yeast mitotic spindle. Nat Cell Biol *8*, 913-923.

Hammond, J.W., Blasius, T.L., Soppina, V., Cai, D., and Verhey, K.J. (2010). Autoinhibition of the kinesin-2 motor KIF17 via dual intramolecular mechanisms. J Cell Biol *189*, 1013-1025.

Hertzer, K.M., Ems-McClung, S.C., Kline-Smith, S.L., Lipkin, T.G., Gilbert, S.P., and Walczak, C.E. (2006). Full-length dimeric MCAK is a more efficient microtubule depolymerase than minimal domain monomeric MCAK. Mol Biol Cell *17*, 700-710.

Honnappa, S., Gouveia, S.M., Weisbrich, A., Damberger, F.F., Bhavesh, N.S., Jawhari, H., Grigoriev, I., van Rijssel, F.J., Buey, R.M., Lawera, A., Jelesarov, I., Winkler, F.K., Wuthrich, K., Akhmanova, A., and Steinmetz, M.O. (2009). An EB1-binding motif acts as a microtubule tip localization signal. Cell *138*, 366-376.

Imanishi, M., Endres, N.F., Gennerich, A., and Vale, R.D. (2006). Autoinhibition regulates the motility of the C. elegans intraflagellar transport motor OSM-3. J Cell Biol *174*, 931-937.

Kalab, P., and Heald, R. (2008). The RanGTP gradient - a GPS for the mitotic spindle. J Cell Sci *121*, 1577-1586.

Kalab, P., Pralle, A., Isacoff, E.Y., Heald, R., and Weis, K. (2006). Analysis of a RanGTP-regulated gradient in mitotic somatic cells. Nature. *440*, 697-701.

Kalab, P., Weis, K., and Heald, R. (2002). Visualization of a Ran-GTP gradient in interphase and mitotic *Xenopus* egg extracts. Science. *295*, 2452-2456.

Kiyomitsu, T., and Cheeseman, I.M. (2012). Chromosome- and spindle-pole-derived signals generate an intrinsic code for spindle position and orientation. Nat Cell Biol *14*, 311-317.

Kosugi, S., Hasebe, M., Matsumura, N., Takashima, H., Miyamoto-Sato, E., Tomita, M., and Yanagawa, H. (2009). Six classes of nuclear localization signals specific to different binding grooves of importin alpha. J Biol Chem *284*, 478-485.

Kristofferson, D., Mitchison, T., and Kirschner, M. (1986). Direct Observation of Steadt-State Microtubule Dynamics. J Cell Biol *102*, 1007-1019.

Lee, Y.M., Kim, E., Park, M., Moon, E., Ahn, S.M., Kim, W., Hwang, K.B., Kim, Y.K., Choi, W., and Kim, W. (2010). Cell cycle-regulated expression and subcellular localization of a kinesin-8 member human KIF18B. Gene *466*, 16-25.

Mayr, M.I., Hummer, S., Bormann, J., Gruner, T., Adio, S., Woehlke, G., and Mayer, T.U. (2007). The human kinesin Kif18A is a motile microtubule depolymerase essential for chromosome congression. Curr Biol *17*, 488-498.

McHugh, T., Gluszek, A.A., and Welburn, J.P.I. (2018). Microtubule end tethering of a processive kinesin-8 motor Kif18b is required for spindle positioning. J Cell Biol *217*, 2403-2416.

Mitchison, T., and Kirschner, M. (1984). Dynamic instability of microtubule growth. Nature. *312*, 237-242.

Moreci, R.S., and Lechler, T. (2021). KIF18B is a cell type-specific regulator of spindle orientation in the epidermis. Mol Biol Cell *32*, ar29 10.1091/mbc.E21-06-0291

Niwa, S., Nakajima, K., Miki, H., Minato, Y., Wang, D., and Hirokawa, N. (2012). KIF19A is a microtubule-depolymerizing kinesin for ciliary length control. Dev Cell *23*, 1167-1175.

Nogales, E., and Zhang, R. (2016). Visualizing microtubule structural transitions and interactions with associated proteins. Curr Opin Struct Biol *37*, 90-96.

Reese, L., Melbinger, A., and Frey, E. (2011). Crowding of molecular motors determines microtubule depolymerization. Biophys J *101*, 2190-2200.

Ribbeck, K., Groen, A.C., Santarella, R., Bohnsack, M.T., Raemaekers, T., Kocher, T., Gentzel, M., Gorlich, D., Wilm, M., Carmeliet, G., Mitchison, T.J., Ellenberg, J., Hoenger, A., and Mattaj, I.W. (2006). NuSAP, a mitotic RanGTP target that stabilizes and cross-links microtubules. Mol Biol Cell. *17*, 2646-2660.

Schatz, C.A., Santarella, R., Hoenger, A., Karsenti, E., Mattaj, I.W., Gruss, O.J., and Carazo-Salas, R.E. (2003a). Importin a-regulated nucleation of microtubules by TPX2. EMBO J *22*, 2060-2070.

Schatz, C.A., Santarella, R., Hoenger, A., Karsenti, E., Mattaj, I.W., Gruss, O.J., and Carazo-Salas, R.E. (2003b). Importin alpha-regulated nucleation of microtubules by TPX2. EMBO J. *22*, 2060-2070.

Shin, Y., Du, Y., Collier, S.E., Ohi, M.D., Lang, M.J., and Ohi, R. (2015). Biased Brownian motion as a mechanism to facilitate nanometer-scale exploration of the microtubule plus end by a kinesin-8. Proc Natl Acad Sci, USA *112*, E3826-3835.

Sillje, H.H., Nagel, S., Korner, R., and Nigg, E.A. (2006). HURP is a Ran-importin beta-regulated protein that stabilizes kinetochore microtubules in the vicinity of chromosomes. Curr Biol *16*, 731-742.

Soderholm, J.F., Bird, S.L., Kalab, P., Sampathkumar, Y., Hasegawa, K., Uehara-Bingen, M., Weis, K., and Heald, R. (2011). Importazole, a small molecule inhibitor of the transport receptor importin-beta. ACS Chem Biol *6*, 700-708.

Steger, C. (1998). An unbiased detector of curvilinear structures. IEEE Trans Pattern Anal Mach Intell *20*, 113-125.

Stout, J.R., Yount, A.L., Powers, J.A., Leblanc, C., Ems-McClung, S.C., and Walczak, C.E. (2011). Kif18B interacts with EB1 and controls astral microtubule length during mitosis. Mol Biol Cell *22*, 3070-3080.

Stumpff, J., Du, Y., English, C.A., Maliga, Z., Wagenbach, M., Asbury, C.L., Wordeman, L., and Ohi, R. (2011). A Tethering Mechanism Controls the Processivity and Kinetochore-Microtubule Plus-End Enrichment of the Kinesin-8 Kif18A. Mol Cell *43*, 764-775.

Stumpff, J., von Dassow, G., Wagenbach, M., Asbury, C., and Wordeman, L. (2008). The kinesin-8 motor Kif18A suppresses kinetochore movements to control mitotic chromosome alignment. Dev Cell *14*, 252-262.

Su, X., Qiu, W., Gupta, M.L., Jr., Pereira-Leal, J.B., Reck-Peterson, S.L., and Pellman, D. (2011). Mechanisms underlying the dual-mode regulation of microtubule dynamics by Kip3/kinesin-8. Mol Cell *43*, 751-763.

Tahara, K., Takagi, M., Ohsugi, M., Sone, T., Nishiumi, F., Maeshima, K., Horiuchi, Y., Tokai-Nishizumi, N., Imamoto, F., Yamamoto, T., Kose, S., and Imamoto, N. (2008). Importin-beta and the small guanosine triphosphatase Ran mediate chromosome loading of the human chromokinesin Kid. J Cell Biol *180*, 493-506.

Tanenbaum, M.E., Macurek, L., van der Vaart, B., Galli, M., Akhmanova, A., and Medema, R.H. (2011). A Complex of Kif18B and MCAK Promotes Microtubule Depolymerization and Is Negatively Regulated by Aurora Kinases. Curr Biol *21*, 1356-1365.

Trieselmann, N., Armstrong, S., Rauw, J., and Wilde, A. (2003). Ran modulates spindle assembly by regulating a subset of TPX2 and Kid activities including Aurora A activation. J Cell Sci *116*, 4791-4798.

van Heesbeen, R., Raaijmakers, J.A., Tanenbaum, M.E., Halim, V.A., Lelieveld, D., Lieftink, C., Heck, A.J.R., Egan, D.A., and Medema, R.H. (2017). Aurora A, MCAK, and Kif18b promote Eg5-independent spindle formation. Chromosoma. *126*, 473-486.

Varga, V., Helenius, J., Tanaka, K., Hyman, A.A., Tanaka, T.U., and Howard, J. (2006). Yeast kinesin-8 depolymerizes microtubules in a length-dependent manner. Nat Cell Biol *8*, 957-962.

Verhey, K.J., and Hammond, J.W. (2009). Traffic control: regulation of kinesin motors. Nat Rev Mol Cell Biol *10*, 765-777.

Walczak, C.E., Gayek, S., and Ohi, R. (2013). Microtubule-Depolymerizing Kinesins. Annu Rev Cell Dev Biol *29*, 417-441.

Walczak, C.E., Zong, H., Jain, S., and Stout, J.R. (2016). Spatial regulation of astral microtubule dynamics by Kif18B in PtK cells. Mol Biol Cell *27*, 3021-3030.

Weaver, L.N., Ems-McClung, S.C., Stout, J.R., LeBlanc, C., Shaw, S.L., Gardner, M.K., and Walczak, C.E. (2011). Kif18A uses a microtubule binding site in the tail for plus-end localization and spindle length regulation. Curr Biol *21*, 1500-1506.

Wiese, C., Wilde, A., Moore, M.S., Adam, S.A., Merdes, A., and Zheng, Y. (2001). Role of importin-beta in coupling Ran to downstream targets in microtubule assembly. Science. *291*, 653-656.

Zheng, Z., Wan, Q., Liu, J., Zhu, H., Chu, X., and Du, Q. (2013). Evidence for dynein and astral microtubule-mediated cortical release and transport of Galphai/LGN/NuMA complex in mitotic cells. Mol Biol Cell *24*, 901-913.

Table S1. Cloning primers

***Clone*/Primer pair**	**Enzyme**	**Sequence 5' to 3'***
pRSETB-EB1-CyPet		
T7 Forward		TAATACGACTCACTATAGGG
EB1 R1	*Xho*I	gat**ctcgag**GCATACTCTTCTTG
pRSETB-YPet-Kif18B(605-828)		
Kif18B(605-828) F1	*Sac*I	c**gagctc**cACCCGGACTATGGCGAG
Kif18B(605-828) R1	*Pst*I	aa**ctgcag**CTAGAGTACAAGGGGCCCAG
pRSETB-YPet-Kif18B(708-828)		
Kif18B(708-828) F1	*Sac*I	gtataa**gagctc**cAAAAGCCGGGTGCCCCTG
Kif18B(708-828) R2	*Pst*I	aa**ctgcag**CTAGAGTACAAGGGGCCCAG
pET24b(+)-YPet-Kif18B(605-828) or pET24b(+)-YPet-Kif18B(708-828)		
YPet-Kif18B(605-628) F1^	*Bam*HI	a**ggatcc***G*ATGGTGAGCAAAGGC
YPet-Kif18B(605-828) R1	*Sal*I	tt**gtcgac**GAGTACAAGGGGCC
pET24b (+)-YPet-Kif18B(605-707)		
YPet-Kif18B(605-628) F1^	*Bam*HI	a**ggatcc***G*ATGGTGAGCAAAGGC
YPet-KIF18B(605-707) R1	*Sal*I	tt**gtcgac**GATGACTGTGGCTGG
pFastBac1-DEST		
attR1-SacI	*Sac*I	gtac**gagctc**GAACAAGTTTGTACAAAAAAGC
attR2-KpnI	*Kpn*I	TTTCTTGTACAAAGTGGTG**ggtacc**ccg
pENTR-EGFP-Kif18B		
pENTR-EGFP F1		CACCATGGTGAGCAAGGGCGAGGA
Kif18B 828 R1		CTAGAGTACAAGGGGCCCAG

*Lowercase and bold bases denote restriction sites, and lowercase bases denote bases added to enhance restriction digestion.

^YPet-Kif18B(605-628) F1 primer recognizes the beginning sequence of YPet, and hence could be used to generate pET24b-YPet-Kif18B(605-828), pET24b-YPet-Kif18B(708-828), and pET24b-YPet-Kif18B(605-707).

Table S2. Mutagenesis primers

Primer name	**Sequence 5' to 3'****
YPet-Kif18B(605-828) NLS1a F	GTCCCGATGGCCCATGGAGgcGgcGgcGAGGAGACCAAGCGC
YPet-Kif18B(605-828) NLS1a R	GCGCTTGGTCTCCTCgcCgcCgcCTCCATGGGCCATCGGGAC
YPet-Kif18B(605-828) NLS1b F	GACAGTCCCATGGCCCCAgcGgcGGGCACCAAGCGCCAGCGC
YPet-Kif18B(605-828) NLS1b R	GCGCTGGCGCTTGGTGCCCgcCgcTGGGGCCATGGGACTGTC
YPet-Kif18B(605-828) NLS2 F	CTGGGACCTCTGCCTGCgcGgcGgcGgcCGTTGCGAGTTCCTCAGTC
YPet-Kif18B(605-828) NLS2 R	GACTGAGGAACTCGCAACGgcCgcCgcCgcGCAGGCAGAGGTCCCAG
YPet-Kif18B(605-828) EB1-E1 F	GCGCCAGCGCCAGTCCTTCaataaCTGCCTAAGGAGAGGGTCTC
YPet-Kif18B(605-828) EB1-E1 R	GAGACCCTCTCCTTAGGCAGttattGAAGGACTGGCGCTGGCGC
YPet-Kif18B(605-828) EB1-E2 F	CCCAAGCCAACATCTTCCaaCaaTGGGACCTCTGCCTGCAAGAAG
YPet-Kif18B(605-828) EB1-E2 R	CTTCTTGCAGGCAGAGGTCCCAttGttGGAAGATGTTGGCTTGGG
YPet-Kif18B(605-828) EB1-E3 F	GCCGCAGCCGCATCGCCCGCaaCaaCAGCAGCACTTTGAAGAGG
YPet-Kif18B(605-828) EB1-E3 R	CCTCTTCAAAGTGCTGCTGttGttGCGGGCGATGCGGCTGCGGC
pENTR-Kif18B-siRNA^{R} F	GCCTCCCTCAAAGCCttccTTCCAcGAgTGCATTGGCTGGG
pENTR-Kif18B-siRNA^{R} R	CCCAGCCAATGCAcTCgTGGAAggaaGGCTTTGAGGGAGGC
pENTR-Kif18B-NLS1a F	GGTCCCGATGGCCCATGGAGg**ctgcag**ccAGGAGACCAAGCGCCTTG GAGGC
pENTR-Kif18B-NLS1a R	GCCTCCAAGGCGCTTGGTCTCCTgg**ctgcag**cCTCCATGGGCCATCGG GACC
pENTR-Kif18B-NLS1b F	GACAGTCCCATGGCCCCAg**ctgcaG**GCACCAAGCGCCAGCGC
pENTR-Kif18B-NLS1b R	GCGCTGGCGCTTGGTGC**Ctgcag**cTGGGGCCATGGGACTGTC
^pENTR-Kif18B-NLS2 F	CTGGGACCTCTGCCTGCgcGgcGgcGgcCGTTGCGAGTTCCTCAGTC
^pENTR-Kif18B-NLS2 R	GACTGAGGAACTCGCAACGgcCgcCgcCgcGCAGGCAGAGGTCCCAG
pENTR-Kif18B-EBBD1 F	GCGCCAGCGCCAGTCCTTCaac**aatT**GCCTAAGGAGAGGGTCTCTGC
pENTR-Kif18B-EBBD1 R	GCAGAGACCCTCTCCTTAGGC**Aatt**gttGAAGGACTGGCGCTGGCGC
pENTR-Kif18B-EBBD3 F	GGCCGCAGCCGCATCGCCCGCaaC**aatt**cCAGCACTTTGAAGAGGCC
pENTR-Kif18B-EBBD3 R	GGCCTCTTCAAAGTGCTGg**aatt**GttGCGGGCGATGCGGCTGCGGCC

** Lowercase bases denote mutated nucleotides and bold bases denote *Pst*I or *MluC*I restriction site introduced for screening.

^These are the same primers as YPet-Kif18B(605-828) NLS2 forward and reverse primers in Table S1

Figures and Legends

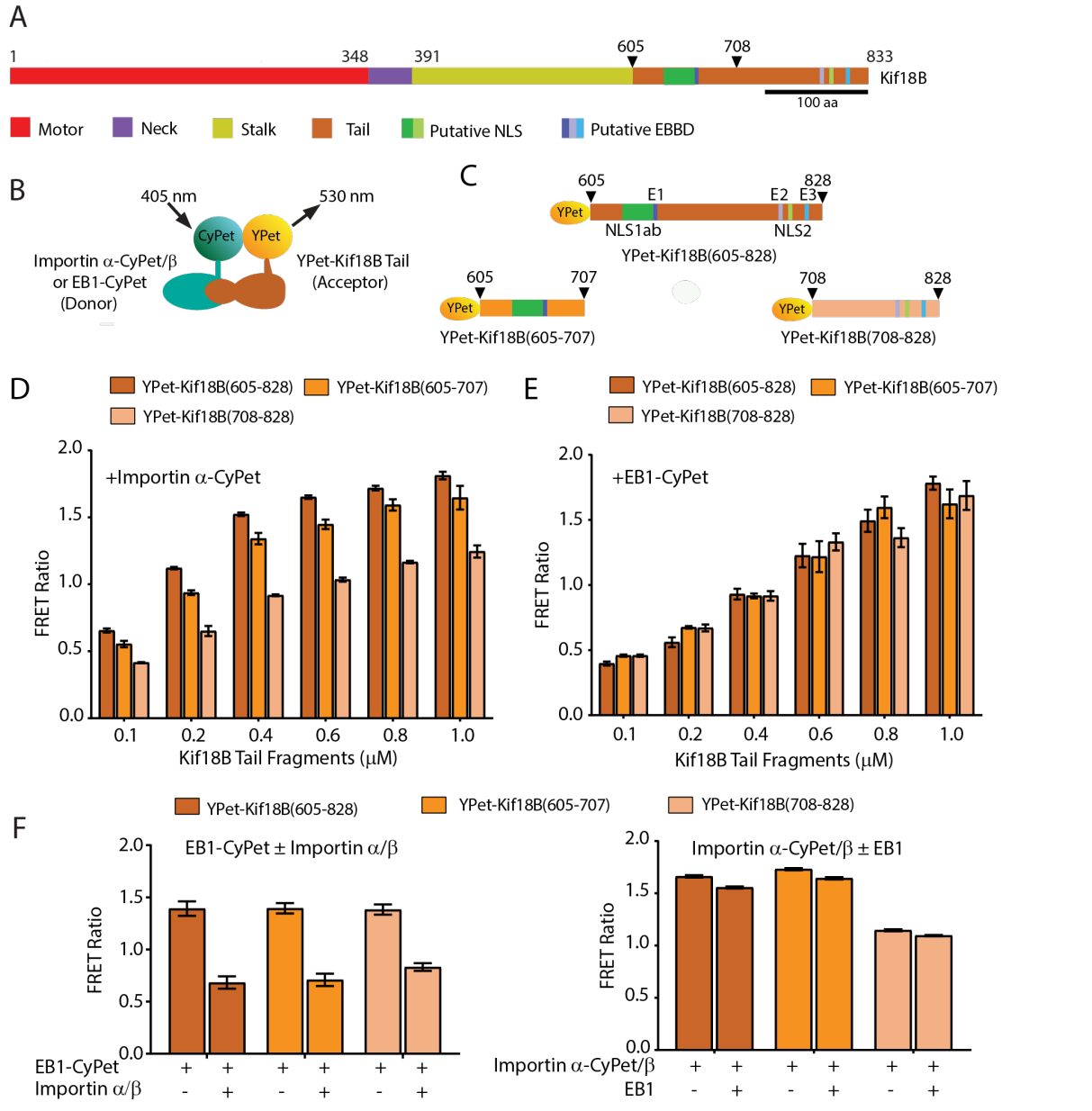

	B_{Max} (μM)	K_d (μM)
YPet-Kif18B(605-828)	0.48	0.14
95% CI	0.41 to 0.56	0.037 to 0.34
YPet-Kif18B(605-828) + Importin α/β	0.39	2.4
95% CI	0.29 to 0.61	1.2 to 5.5

	B_{Max} (μM)	K_d (μM)
YPet-Kif18B(605-828)	0.46	0.063
95% CI	0.43 to 0.49	0.028 to 0.11
YPet-Kif18B(605-828) + EB1	0.49	0.11
95% CI	0.47 to 0.51	0.072 to 0.15

Figure 1. Importin α/β competes with EB1 for binding to Kif18B tail and impairs its microtubule binding. (A) Schematic of full-length human Kif18B showing its domain organization and putative NLS (green) and EB1-binding domains (EBBD) (blue). The arrowheads indicate the beginning residues of the truncated Kif18B proteins used in this study. Scale bar, 100 amino acids (aa). (B) Schematic of FRET between importin α-CyPet/β or EB1-CyPet and YPet-Kif18B tail fragments. (C) Schematics of constructs used in this study with the beginning and ending residues of the truncated proteins indicated, and the NLS and EBBD sites marked as in (A). (D and E) Reactions containing 100 nM importin α-CyPet and 400 nM importin β (D) or 100 nM EB1-CyPet (E) were incubated with increasing concentrations of the three different YPet-Kif18B tail proteins and measured for FRET. The normalized FRET ratios at 530 nm are plotted as the mean ± SEM from three independent experiments. (F) Competition experiments with 800 nM YPet-Kif18B tail fragments were performed between 100 nM EB1-CyPet and 400 nM unlabeled importin α/β (left) or between 100 nM importin α-CyPet/importin β and 400 nM unlabeled EB1 (right) in three independent experiments. FRET was measured, and the normalized FRET ratios graphed as in (D). (G) YPet-Kif18B(605-828) was incubated with increasing concentrations of MTs in the presence or absence of importin α/β (left) or EB1 (right). The fluorescence of YPet in the supernatant and pellet samples was measured, and the fractional binding of YPet-Kif18B(605-828) in molarity was calculated from at least three independent experiments. The normalized data was plotted as the mean ± SEM and fit to the quadratic binding equation.

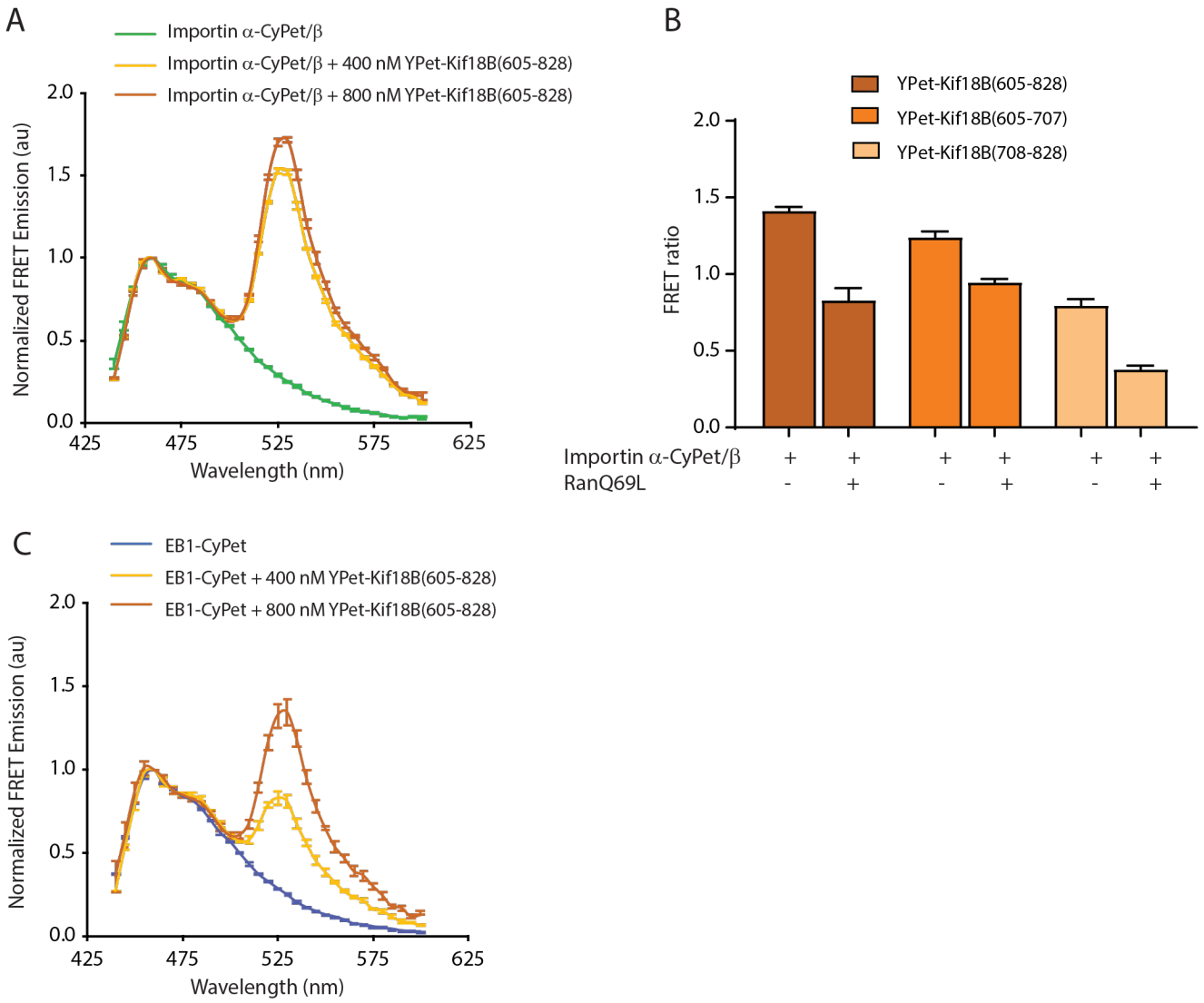

Figure S1. Kif18B undergoes intermolecular FRET with importin a/β or EB1 in a dose dependent manner. Reactions containing 100 nM importin α-CyPet and 400 nM importin β (A) were incubated with 400 or 800 nM YPet-Kif18B(605-828), excited at 405 nm, and their spectral emissions recorded from 440 to 600 nm in 5 nm steps. (B) Reactions containing 100 nM importin α-CyPet and 400 nM importin β with 400 nM YPet-Kif18B tail proteins were measured for FRET as in (A) and then incubated with 10 μM RanQ69L for 10 min and their FRET re-measured. The mean FRET ratio ± SEM before and after RanQ69L addition are plotted. (C) 100 nM of EB1-CyPet (B) was incubated with 400 or 800 nM of YPet-Kif18B(605-828) and the FRET measured as in (A). (A and C) The average normalized spectral emissions from three independent experiments are graphed as the mean ± SEM.

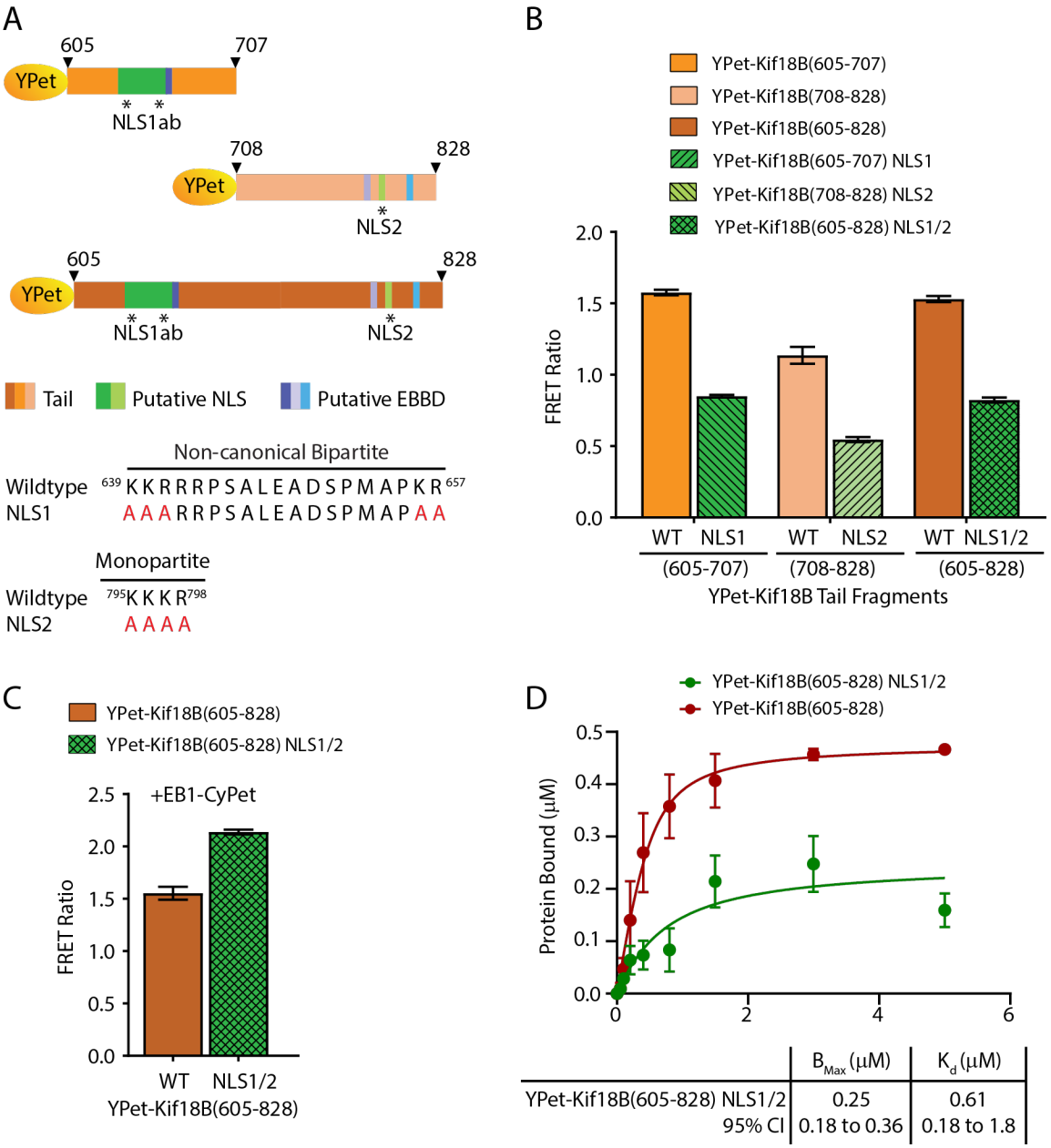

	B_{Max} (μM)	K_d (μM)
YPet-Kif18B(605-828) NLS1/2	0.25	0.61
95% CI	0.18 to 0.36	0.18 to 1.8

Figure 2. Importin α/β interact with the Kif18B tail through a non-canonical bipartite (NLS1) and a monopartite NLS (NLS2). (A) Schematics of the constructs and mutations (indicated by asterisks) used to identify the critical residues in the Kif18B tail required for importin α/β binding. The wildtype amino acid sequences of Kif18B at the two predicted NLS sites are shown with the mutations introduced at the corresponding residues in red. (B) Normalized FRET ratios following the incubation of 100 nM importin a-CyPet with 400nM importin β and 800 nM wildtype or NLS mutant YPet-Kif18B tail fragments. FRET measurements were performed from three independent experiments and plotted as described in Figure 1D. (C) Normalized FRET ratios of 100 nM EB1-CyPet and 800nM YPet-Kif18B(605-828) or YPet-Kif18B(605-828) NLS1/2. The FRET ratios were measured from three independent experiments and plotted as described in Figure 1D. (D) YPet-Kif18B(605-828) NLS1/2 was incubated with increasing concentrations of MTs and the fractional binding was determined from at least three independent experiments as described in Figure 1G. YPet-Kif18B(605-828) fractional binding from Figure 1G (left) is included for comparison.

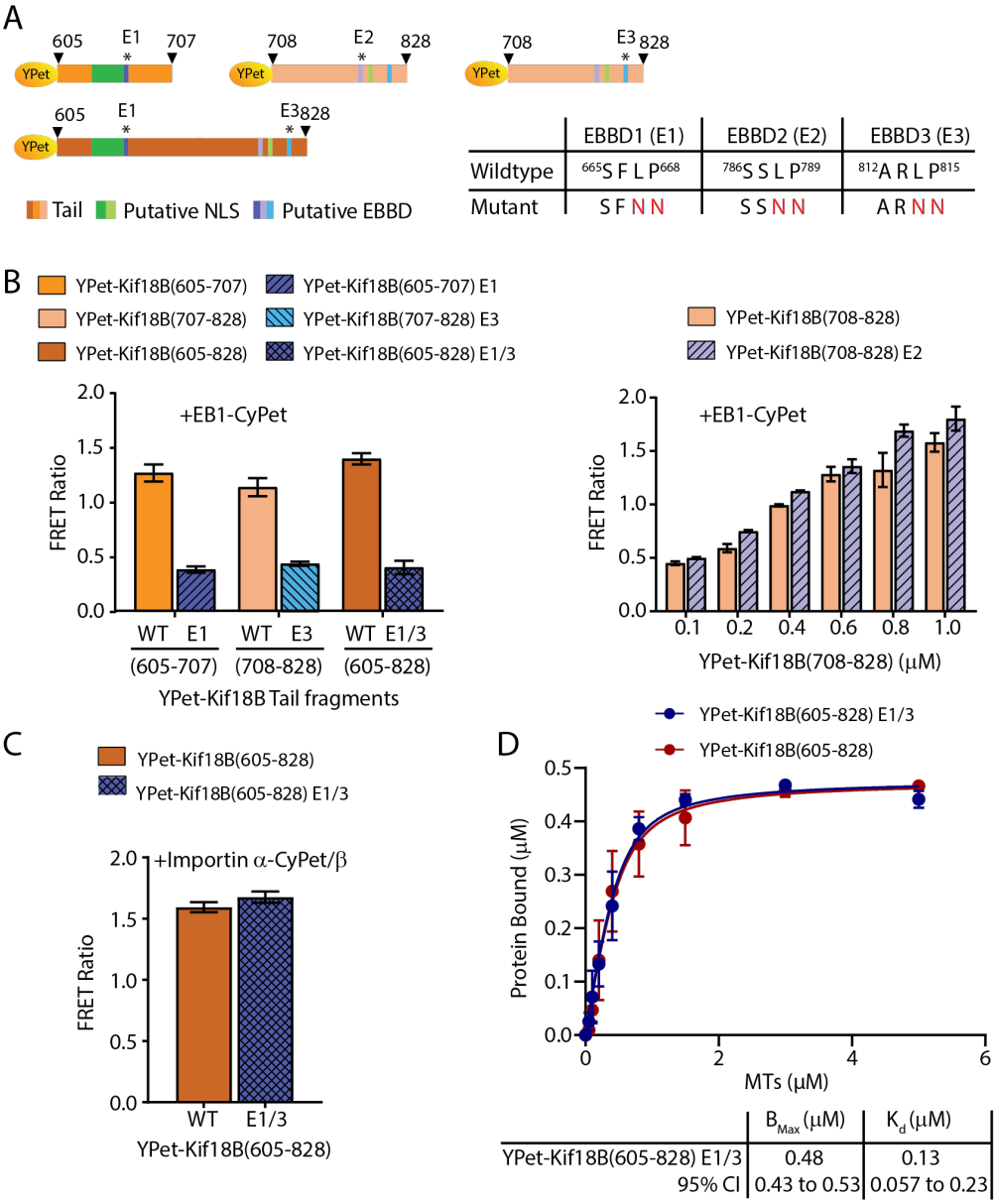

	EBBD1 (E1)	EBBD2 (E2)	EBBD3 (E3)
Wildtype	^{665}S F L P^{668}	^{786}S S L P^{789}	^{812}A R L P^{815}
Mutant	S F N N	S S N N	A R N N

	B_{Max} (μM)	K_d (μM)
YPet-Kif18B(605-828) E1/3	0.48	0.13
95% CI	0.43 to 0.53	0.057 to 0.23

Figure 3. EB1 interacts with Kif18B through two EB1 binding sites in the Kif18B tail. (A) Schematic representations of the constructs and mutations used to map the critical residues needed for EB1 binding where the numbers indicate the residues of Kif18B, and asterisks indicate the mutation sites. The wildtype amino acid sequences of the three putative EB1 binding sites (E1, E2, and E3) and the corresponding mutant sequences are shown with the mutated residues in red. (B) Normalized FRET ratios obtained following incubation of 100 nM EB1-CyPet with 800 nM wildtype or mutant YPet-Kif18B(605-707) E1, YPet-Kif18B(708-828) E3, or YPet-Kif18B(605-828) E1/3 (left). Normalized FRET ratios obtained after incubating 100 nM EB1-CyPet with varying concentrations of wildtype or mutant YPet-Kif18B(708-828) E2 (right). (C) Normalized FRET ratios of 100 nM importin α-CyPet and 400 nM importin β incubated with 800 nM wildtype or mutant YPet-Kif18B(605-828) E1/3. (B and C) FRET ratios were determined from three independent experiments and plotted as in Figure 1D. (D) YPet-Kif18B(605-828) E1/3 was incubated with increasing amounts of MTs to determine fractional binding from at least three independent experiments and was processed as described in Figure 1G. YPet-Kif18B(605-828) fractional binding from Figure 1G (left) is included for comparison.

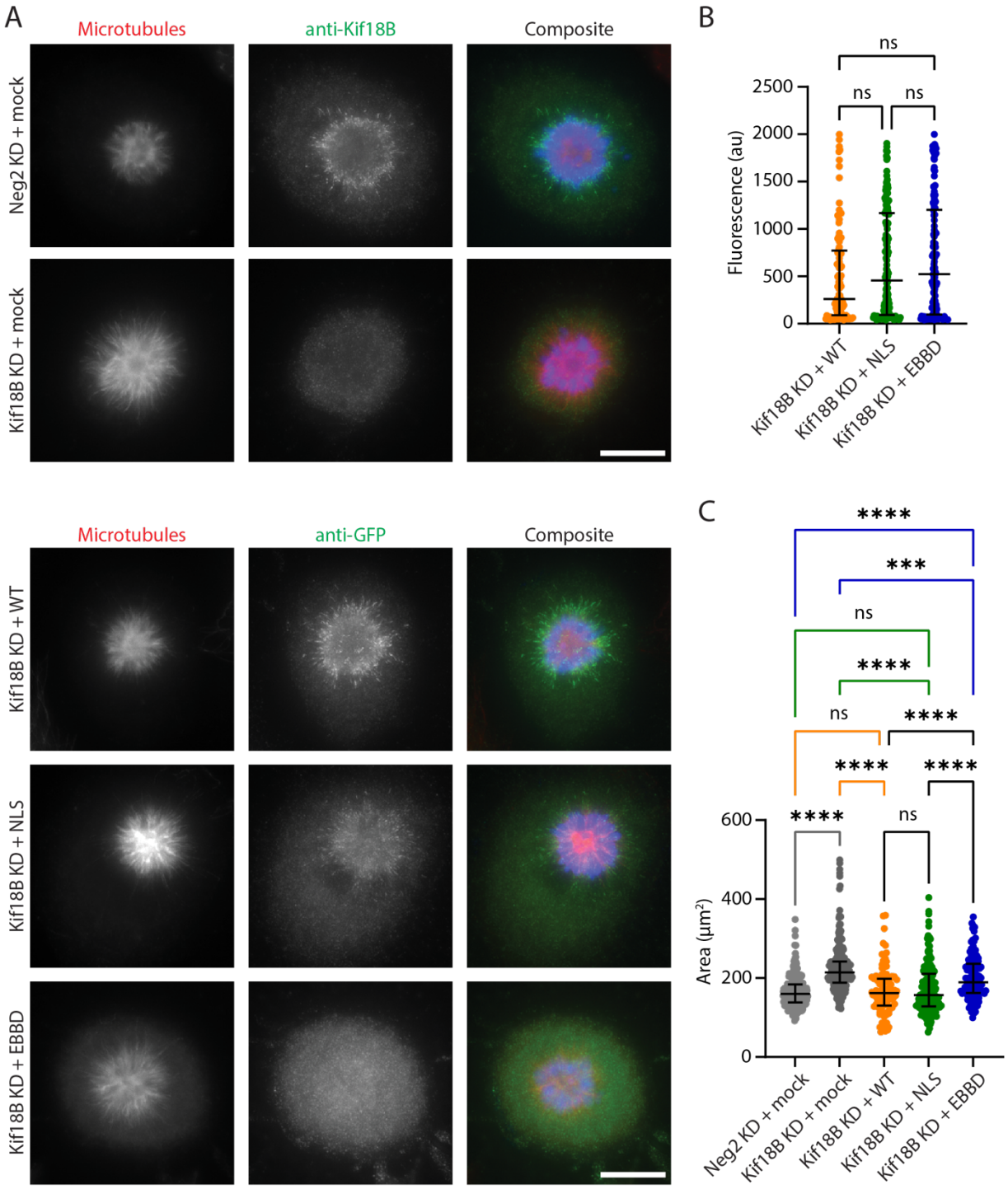

Figure 4. Mutation of the EBBD impacts the ability of Kif18B to control MT length. (A) Cells treated with control Neg2 or Kif18B siRNAs were mock transduced or transduced with WT or mutant lentiviruses, and then fixed and stained for MTs (red), Kif18B (green) or GFP (green), and DNA (blue). Scale bar, 10 µm. (B) The average GFP fluorescence is reported from at least 100 cells from three independent experiments in which each dot represents a single cell, and the median ± interquartile range is indicated. (C) The average MT aster area is reported from the cells in (B) with the median ± interquartile range indicated. ns, not significant; ***, $p<0.001$; ****, $p<0.0001$.

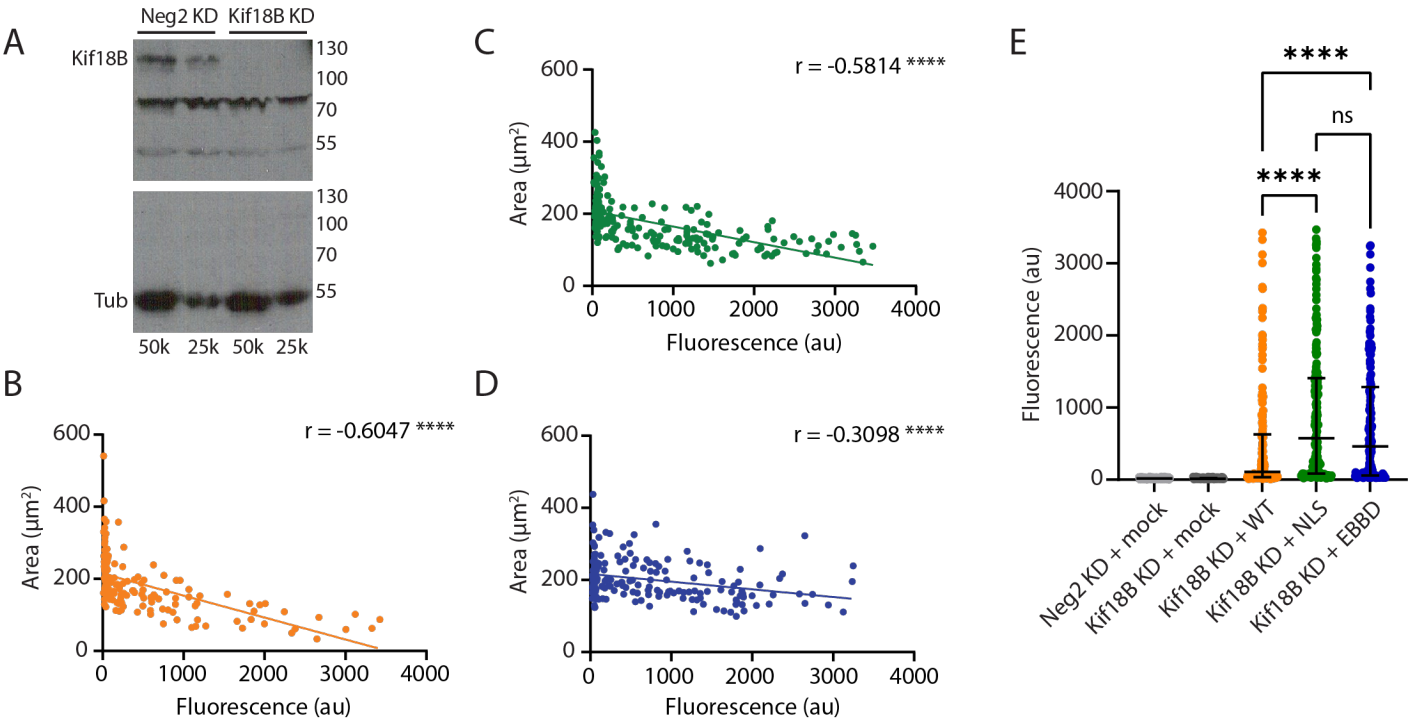

Figure S2. Analysis of GFP expression levels versus aster area. (A) Western blots of control Neg2 knockdown cells (Neg2 KD) or Kif18B knockdown cells (Kif18B KD) probed with an anti-Kif18B antibody (top) or α-tubulin antibody as a loading control (bottom). The number of cells loaded in each lane is indicated at the bottom of the gel. (B-D) Correlation between the aster area vs. GFP fluorescence intensity for all cells measured in Figure 4 expressing WT GFP-Kif18B (B), GFP-Kif18B NLS (C) or GFP-Kif18B EBBD (D). (E) Dot plots showing the individual expression level of GFP in all cells measured for analysis of aster area. This data is before binning for equivalent expression levels between constructs as shown in Figure 4.

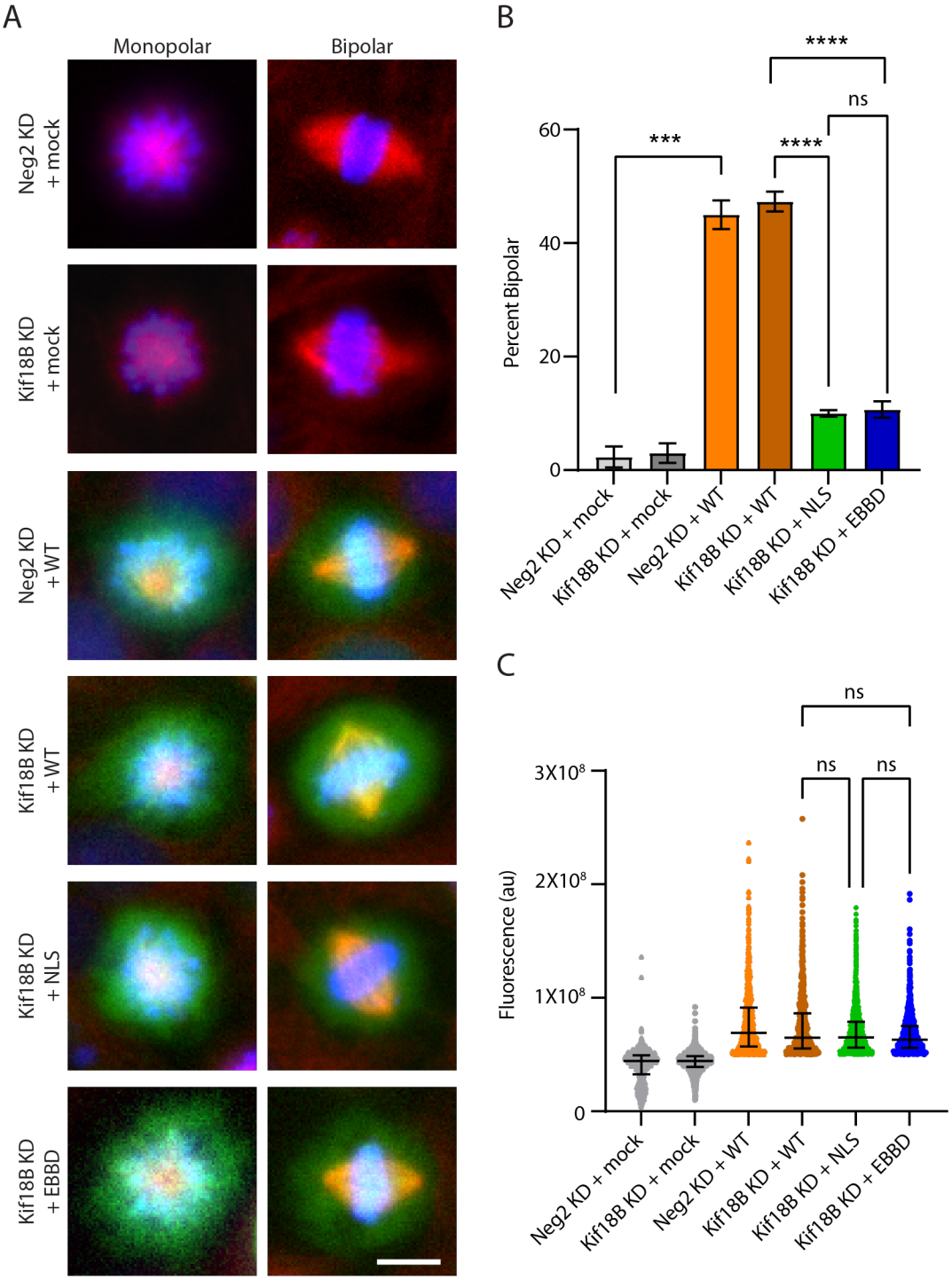

Figure 5. Mutation of the NLS or the EBBD impact bipolar spindle formation. (A) Cells treated with control (Neg2) or Kif18B siRNAs were mock transduced or transduced with WT or mutant lentiviruses, and then fixed and stained for MTs (red) and DNA (blue). Scale bar, 10 μm. (B) The percentage of bipolar spindles were determined by scoring 100 GFP-expressing mitotic cells in three independent experiments with the mean ± SEM indicated. (C) The total GFP fluorescence within 6 μm of the primary mask was calculated with an automated pipeline from three independent experiments. A minimum intensity of $5X10^7$ au was used to define GFP-Kif18B expressing cells. Each dot represents a single cell, and the median ± interquartile range is indicated. ns, not significant; ***, $p<0.001$; ****, $p<0.0001$.

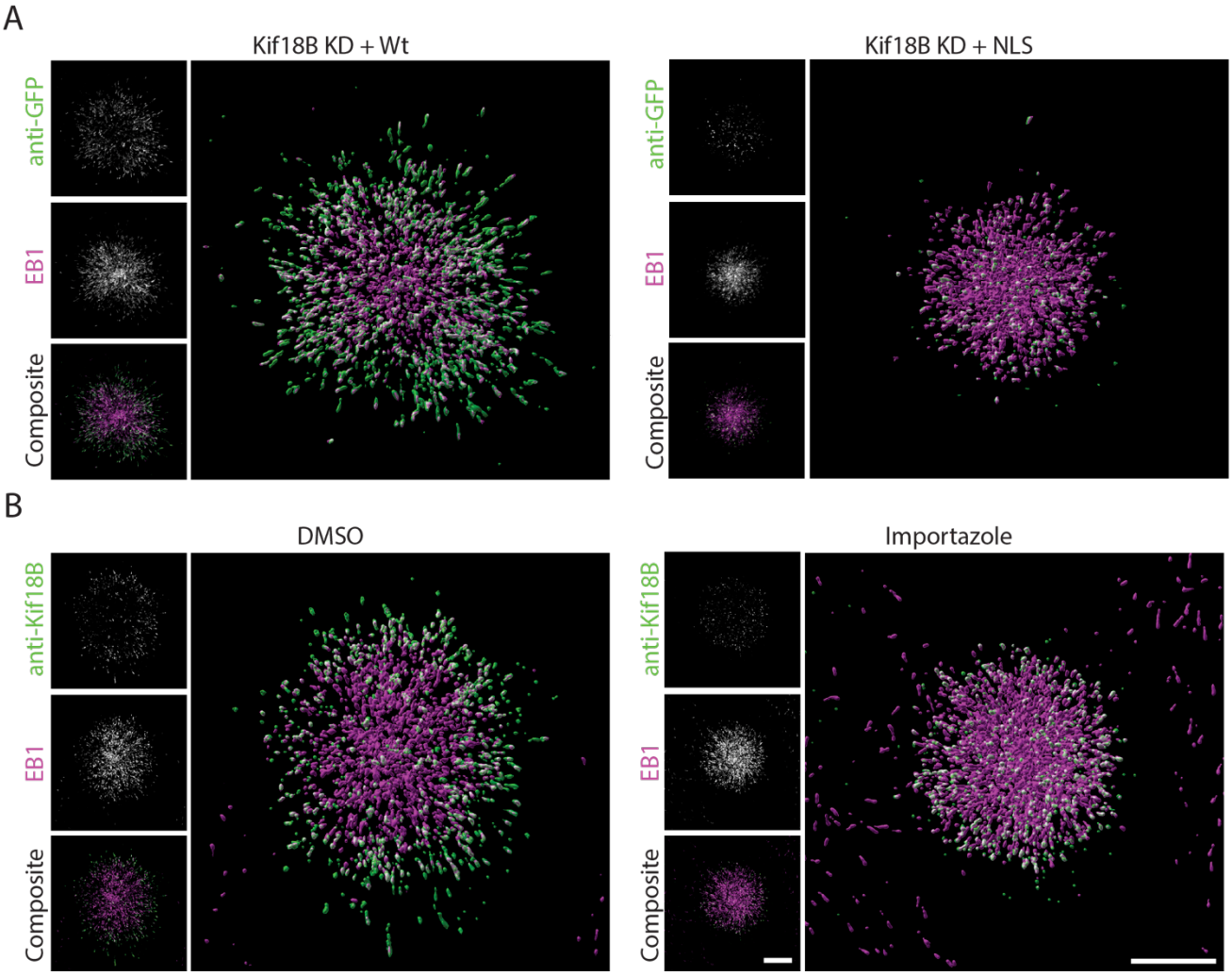

Figure S3. Kif18B knockdown and lentiviral rescue with GFP-Kif18B NLS or importazole treatment disrupts Kif18B localization to the plus ends of MTs. (A) Monastrol treated cells depleted of Kif18B and rescued with WT GFP-Kif18B (left) or with GFP-Kif18B NLS (right) stained with anti-GFP (green) and anti-EB1 (magenta). (B) Monastrol treated cells with DMSO (left) or importazole (right) and stained with anti-Kif18B (green) or anti-EB1 (magenta). Scale bars, 5 μm.

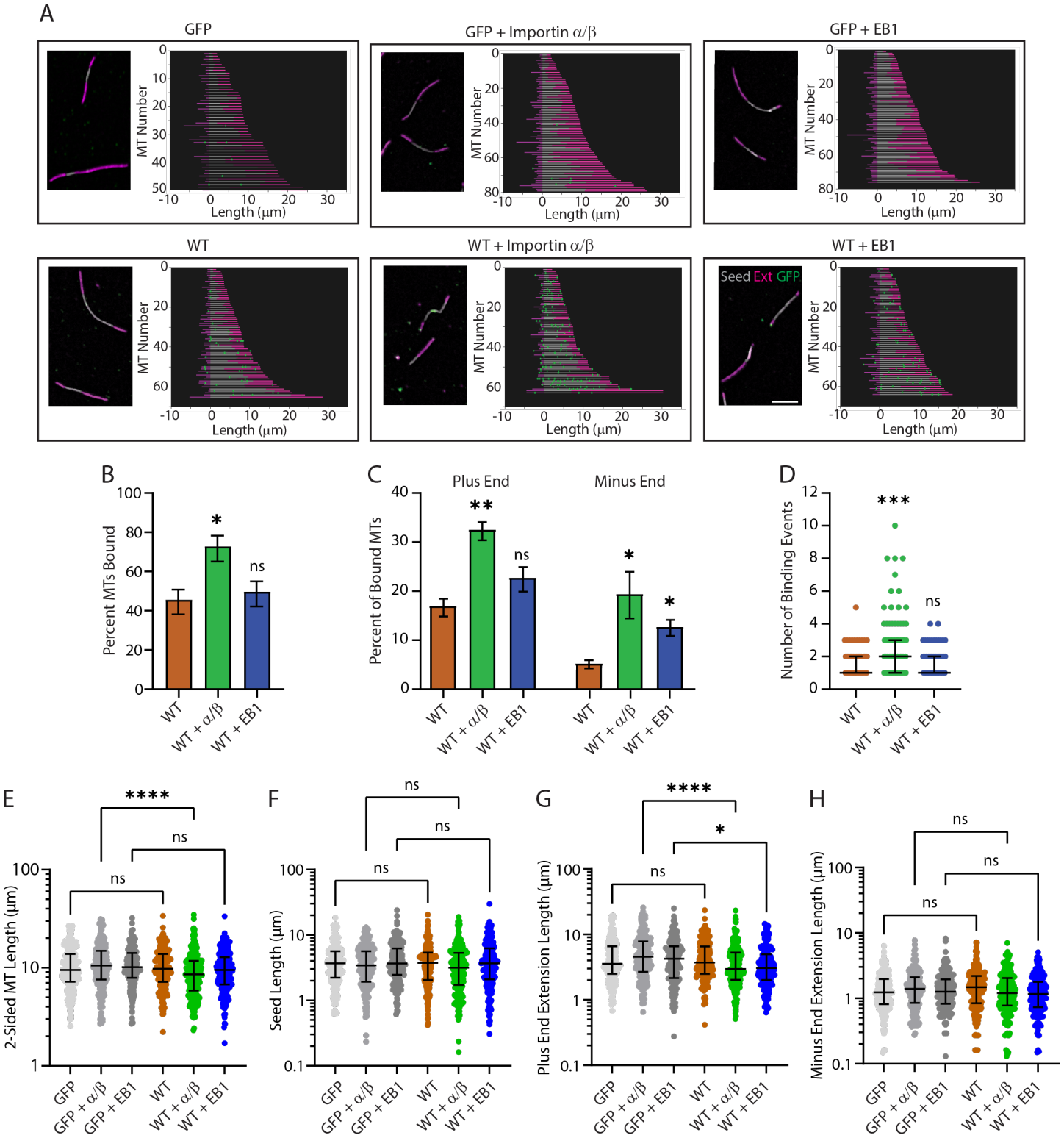

Figure 6. Importin α/β increase Kif18B plus end MT binding and stimulate its MT destabilization activity *in vitro*. (A) X-rhodamine labeled dynamic MTs (magenta) were nucleated from GMPCPP stabilized Cy5 MT seeds (gray) in the presence of 75 nM GFP or GFP-Kif18B ± 300 nM importin α/β or EB1, sedimented onto coverslips, and stained with anti-GFP antibody (green). GFP-Kif18B motor binding events and MT lengths were analyzed using a custom-built MATLAB algorithm. Representative 2-sided MT images (left) and all the 2-sided MTs analyzed with the algorithm (right) from one of three experiments. Scale bar, 10 μm. (B) The percentage of MTs with GFP-Kif18B binding were determined from each experiment and graphed as the mean

± SEM. An unpaired Student's *t*-test was performed to compare the means. (C) The percentage of bound MTs with GFP-Kif18B binding events on the distal plus or minus ends were graphed from each experiment as the mean ± SEM. An unpaired multiple *t*-test was performed to compare the means. (D) Of the MTs with GFP-Kif18B motor binding events, the number of events per MT was determined and graphed from all three experiments with the indicated median ± interquartile range. An ANOVA with Kruskal-Wallis and Dunn's multiple comparisons test was performed to compare the medians. (E-H) The lengths of the 2-sided MTs (E), seeds (F), plus end extensions (G), and minus end extensions (H) were plotted for each MT on a log scale to better represent the lognormal distribution with the median ± interquartile range. A Kruskal-Wallis ANOVA with Dunn's multiple comparisons test was performed to compare the medians. The number of MTs scored for MT binding and length per condition was 175-248. ns, not significant; *, $p<0.05$; **, $p<0.01$; ***, $p<0.001$; ****, $p<0.0001$.

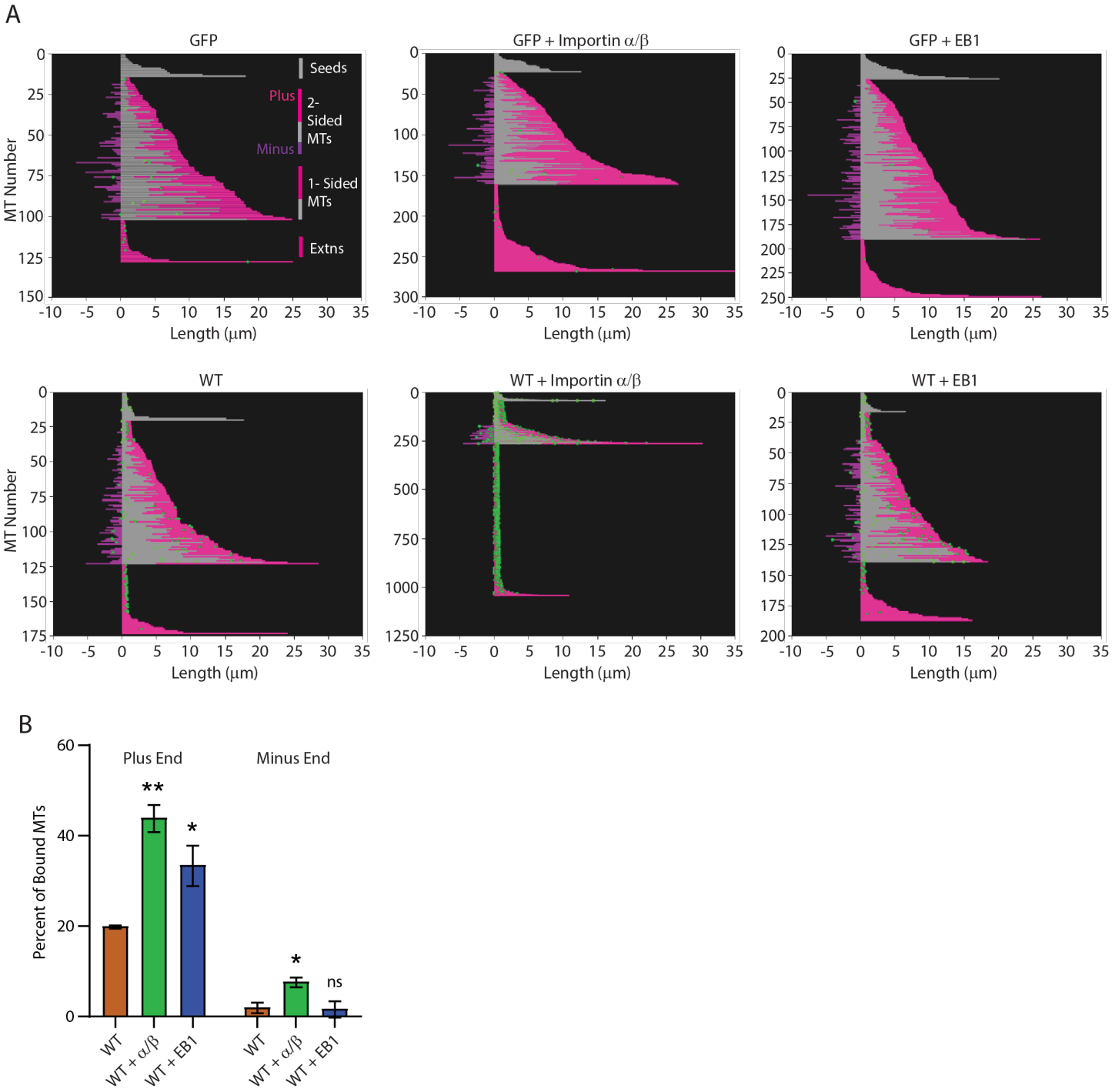

Figure S4. EB1 has increased distal MT plus-end binding after re-categorization of MT lengths. (A) Complete data sets for each condition of a representative experiment analyzed by the custom-built MATLAB algorithm for GFP-Kif18B MT binding and length determination represented in Figure 6 where seeds are gray, plus end extensions are magenta, and minus end extensions are dark purple. (B) MTs with minus end binding events were re-scored as plus end binding events if the longer extension was within 90% of the length of control GFP minus end lengths or 2.7 μm. The resulting adjusted percentage of plus end and minus end binding is plotted from the three independent experiments as the mean ± SEM. A multiple *t*-test was performed to compare the means. ns, not significant; *, $p<0.05$; **, $p<0.01$.

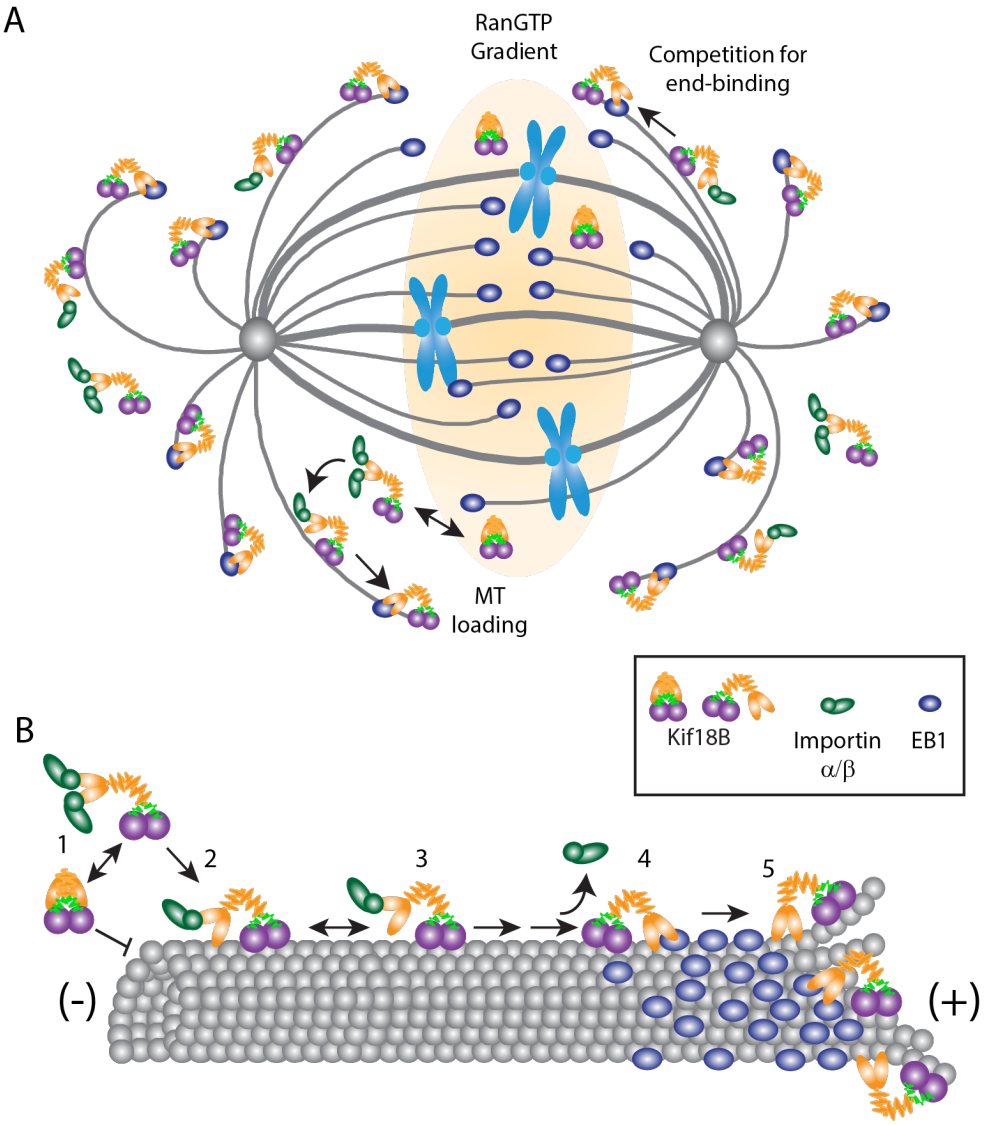

Figure 7. Importin α/β and EB1 differentially regulate Kif18B localization and MT destabilization activity. (A) We propose that near the chromosomes, high RanGTP prevents importin α/β interaction with the tail of Kif18B, preventing Kif18B MT binding. Away from the chromatin where RanGTP levels are low, importin α/β can interact with the tail of Kif18B promoting Kif18B MT association and translocation to the plus ends (MT loading). At MT plus-ends where EB1 accumulates, there is competition between MT bound EB1 and importin α/β that favors Kif18B tail association with EB1 allowing Kif18B to accumulate for the modulation of MT dynamics (Competition for end-binding). (B) We propose the tail of Kif18B autoinhibits the motor domain from robust MT association (1). Importin α/β binding to the tail releases the autoinhibition, allowing the Kif18B motor domain to associate with MTs, which is facilitated by tail-MT binding (2). Tail mediated binding and unbinding to MTs and/or importin α/β facilitates directed plus-end motility (3). Upon encountering a comet of EB1 on the MT plus-end, EB1 competes with the importins and/or MTs for tail association that facilitates Kif18B to accumulate at the MT plus tips (4) where it can be positioned for MT destabilization (5).